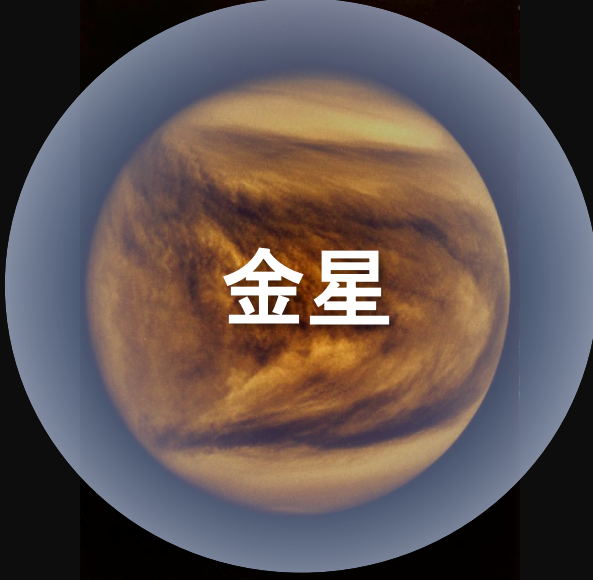


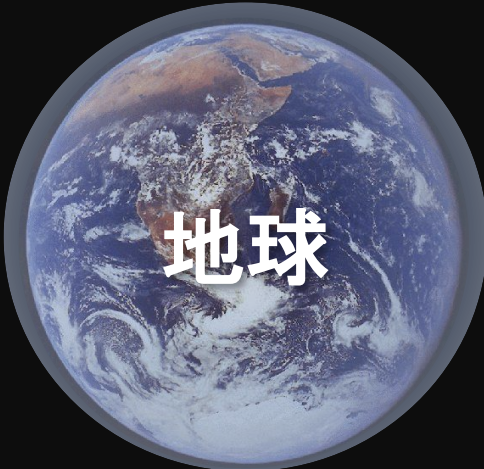
# 惑星大気の散逸と変遷

# 温室効果がもたらす気候の違い



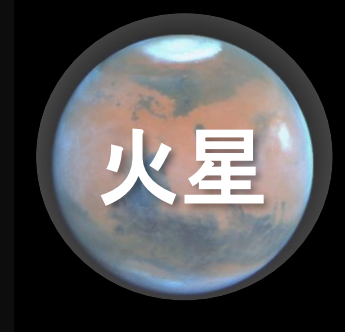
濃い二酸化炭素  
の大気

灼熱の星  
( $460^{\circ}\text{C}$ )



水蒸気と、ほどよい  
量の二酸化炭素

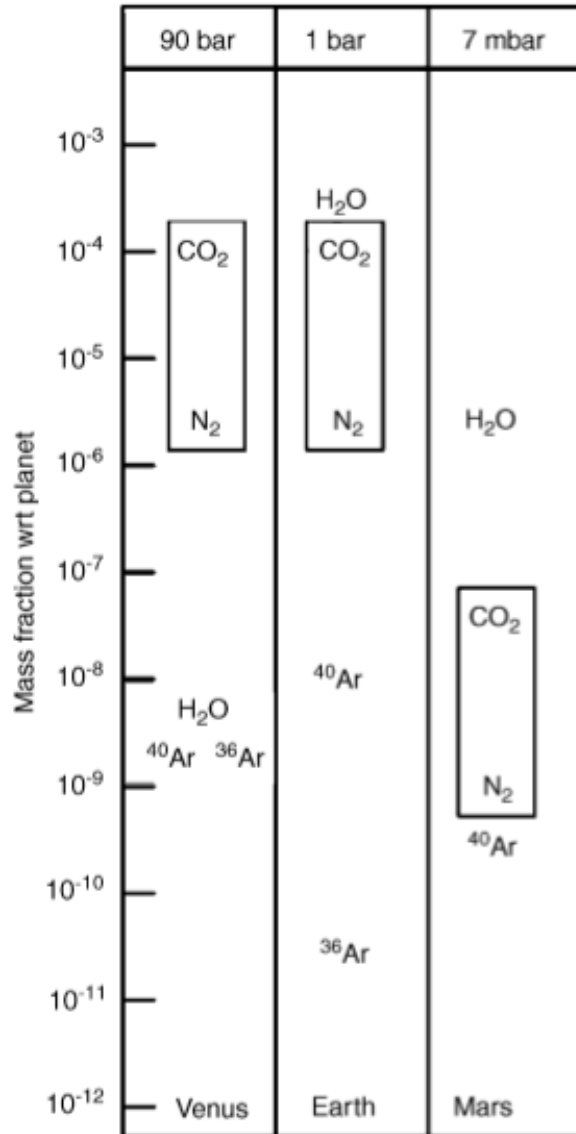
生命の星  
( $15^{\circ}\text{C}$ )



とても薄い大気

凍りついた星  
( $-60^{\circ}\text{C}$ )

# 地球型惑星の揮発性物質



- 金星では $\text{H}_2\text{O}$ が地球・火星に比べて極端に少ない。→金星の $\text{H}_2\text{O}$ は散逸で失われたか
- 火星の $\text{CO}_2$ ,  $\text{N}_2$ は地球・金星の値の1/1000以下。一方、惑星形成後しばらくして脱ガスしたと考えられる $^{40}\text{Ar}$ はそれほど変わらない。→火星の $\text{CO}_2$ ,  $\text{N}_2$ は形成直後に大量散逸か

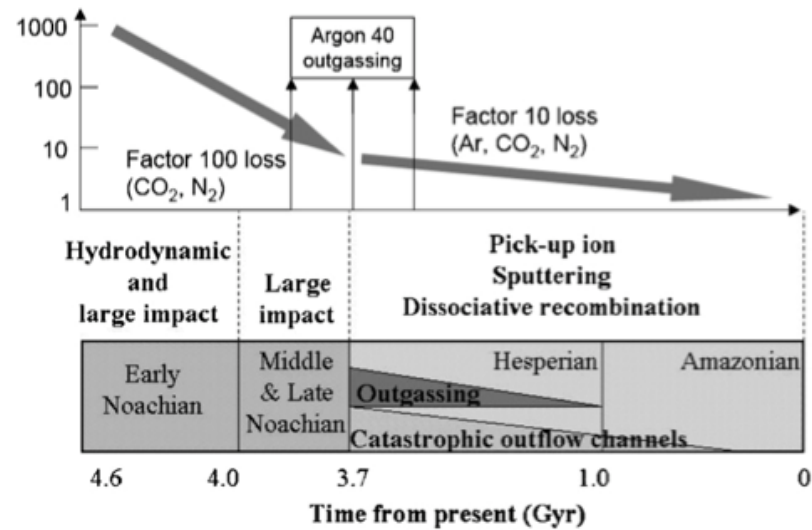


Fig. 1. Mass fraction with respect to planetary mass of volatiles on the terrestrial planets (by taking into account all known reservoirs, in particular terrestrial carbonates for  $\text{CO}_2$ ).

Chassefiere et al. (2007)

Fig. 3. Schematic chronology of atmospheric escape on Mars. A factor of 100 loss is expected to have occurred during the heavy bombardment period, by impact loss and possibly hydrodynamic escape. In the subsequent period, by using radiogenic argon as a tracer of sputtering escape, an additional loss by a typical factor of 10 occurred.

# 大気の散逸

## 熱的散逸 Thermal escape

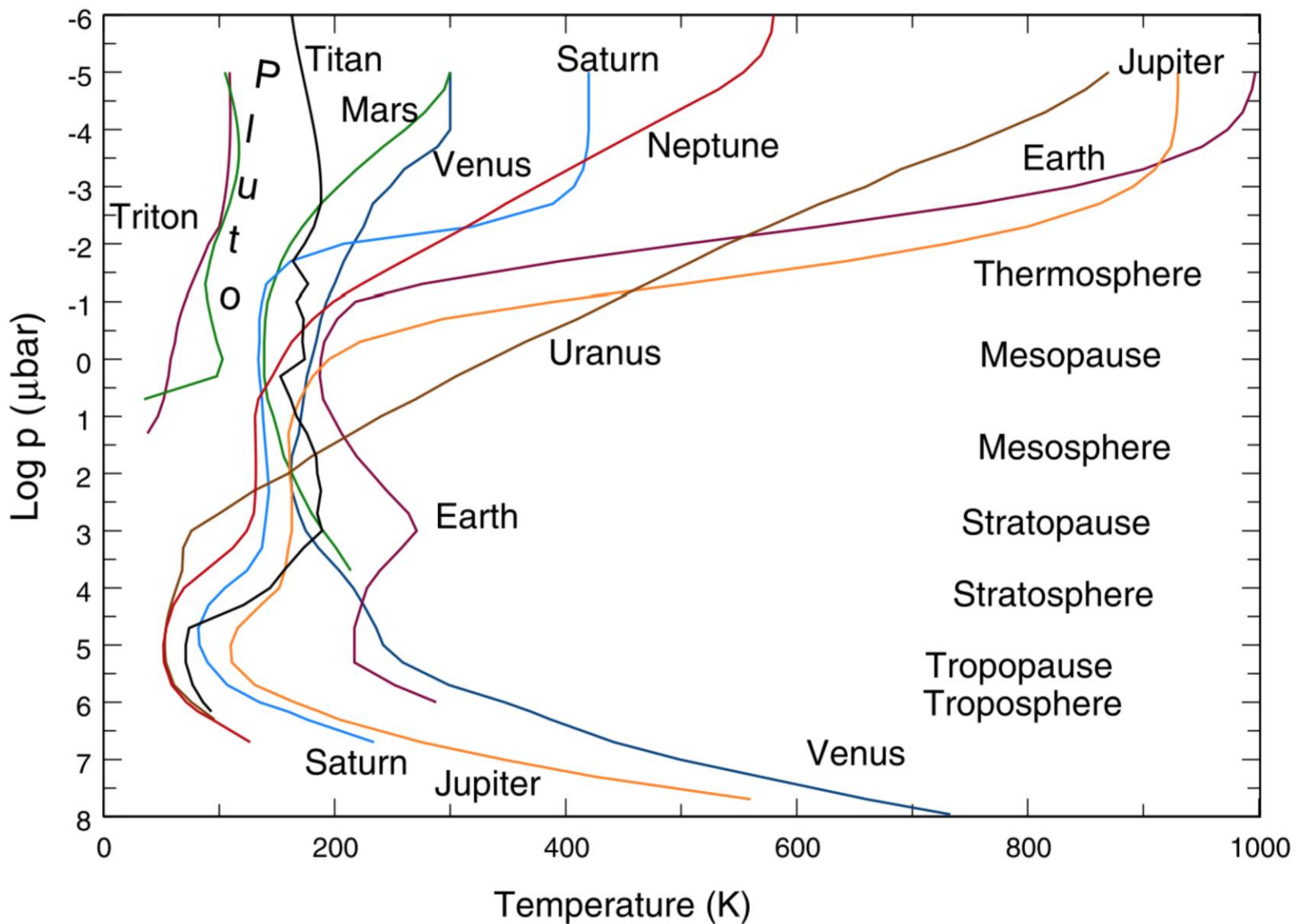
- Hydrodynamic escape
  - 上層大気(熱圏)が太陽のEUV(extreme-ultraviolet)放射で加熱されて高温になる、あるいは水素など軽いガスが上層大気の多くを占めることにより、大気が高い高度まで広がると、外向きの圧力勾配と内向きの重力をバランスさせることができずに圧力勾配によって大気が流体的に流れ出す。
- Jeans' escape
  - ある割合の分子は統計的に必ず脱出速度を超えており、分子間衝突の少ない外圏(exosphere)ではこれらの分子は宇宙空間に散逸する。

## 非熱的散逸 Nonthermal escape

- 解離的再結合、charge exchange, pick-up, sputteringなど
  - 大気中の化学反応や太陽風の効果により高いエネルギーを得た分子が散逸する。
  - 一般にhydrodynamic escapeより長期にわたって続くことが予想される。

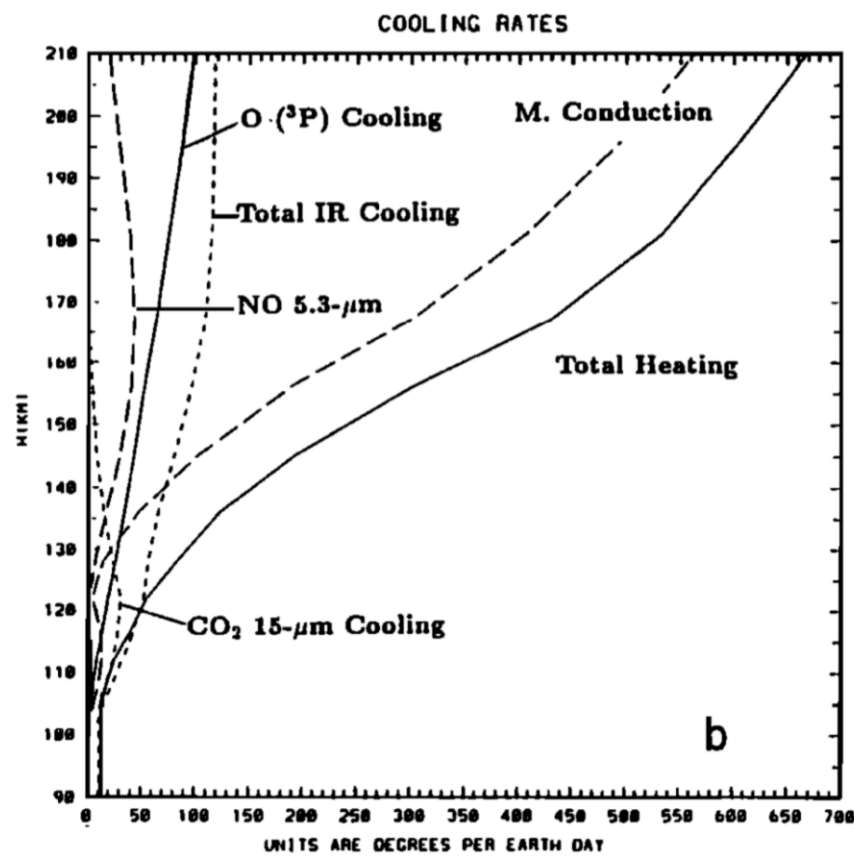
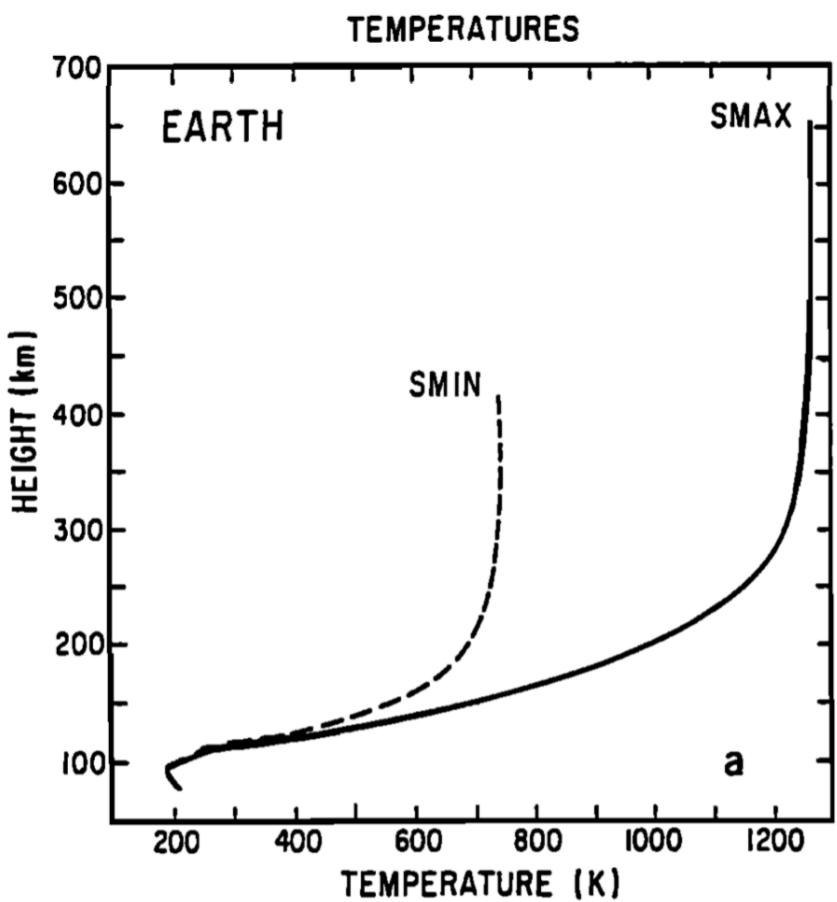
# 惑星大気の温度構造

(Mueller-Wodarg et al.)

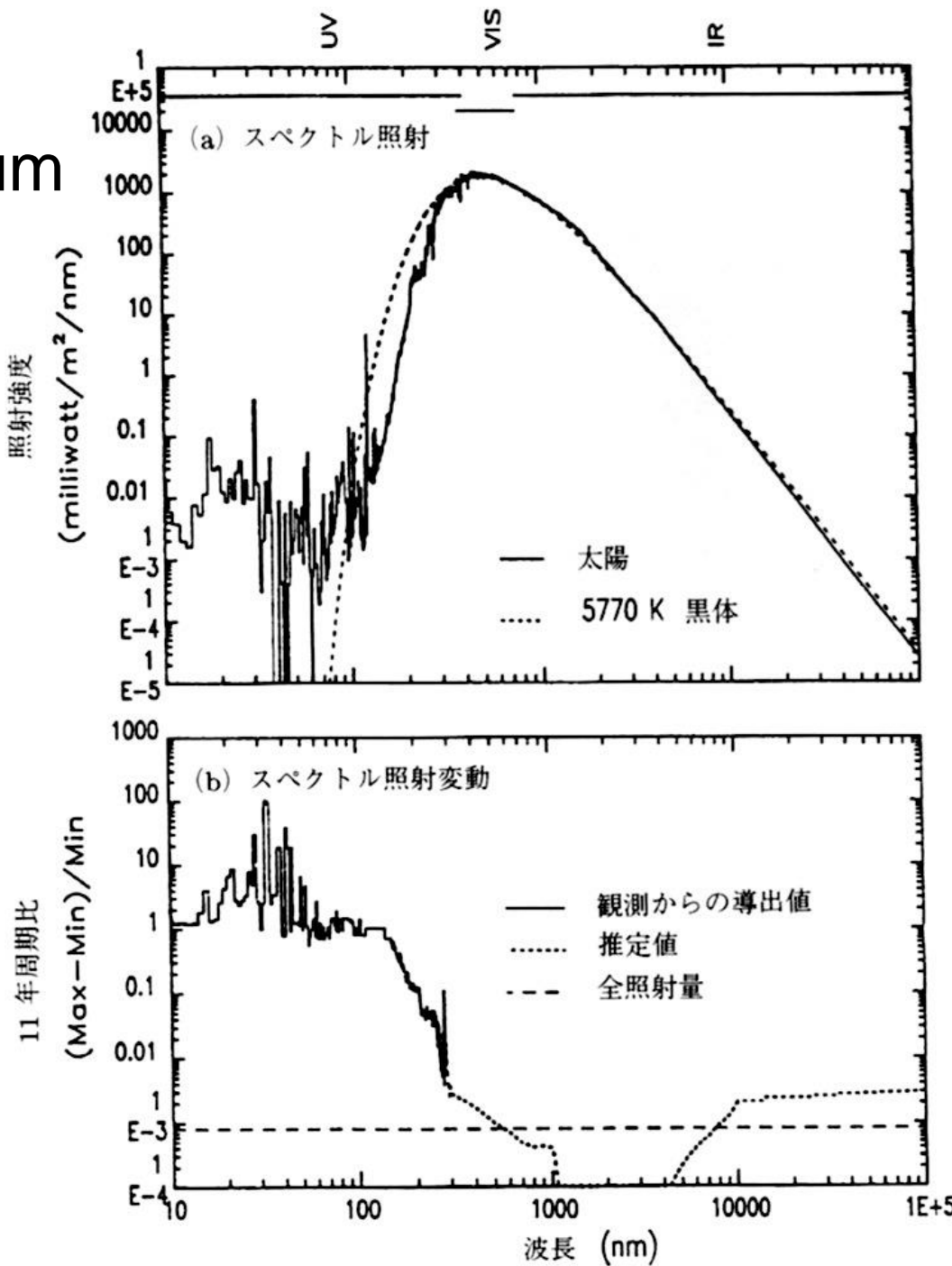


# 熱巻のエネルギーバランス：紫外加熱と熱伝導

(Bougher et al. 1994)



# Solar spectrum



(ブレッケ, 超高層  
大気物理学)

# Source of solar EUV

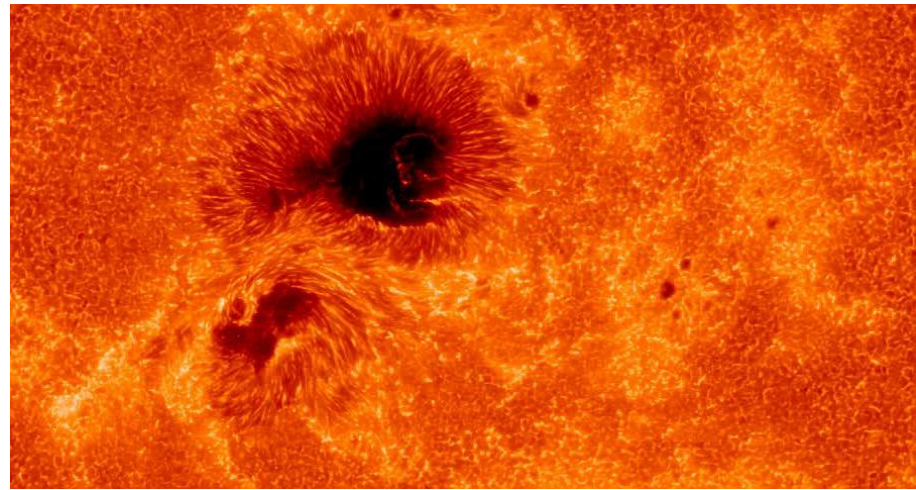
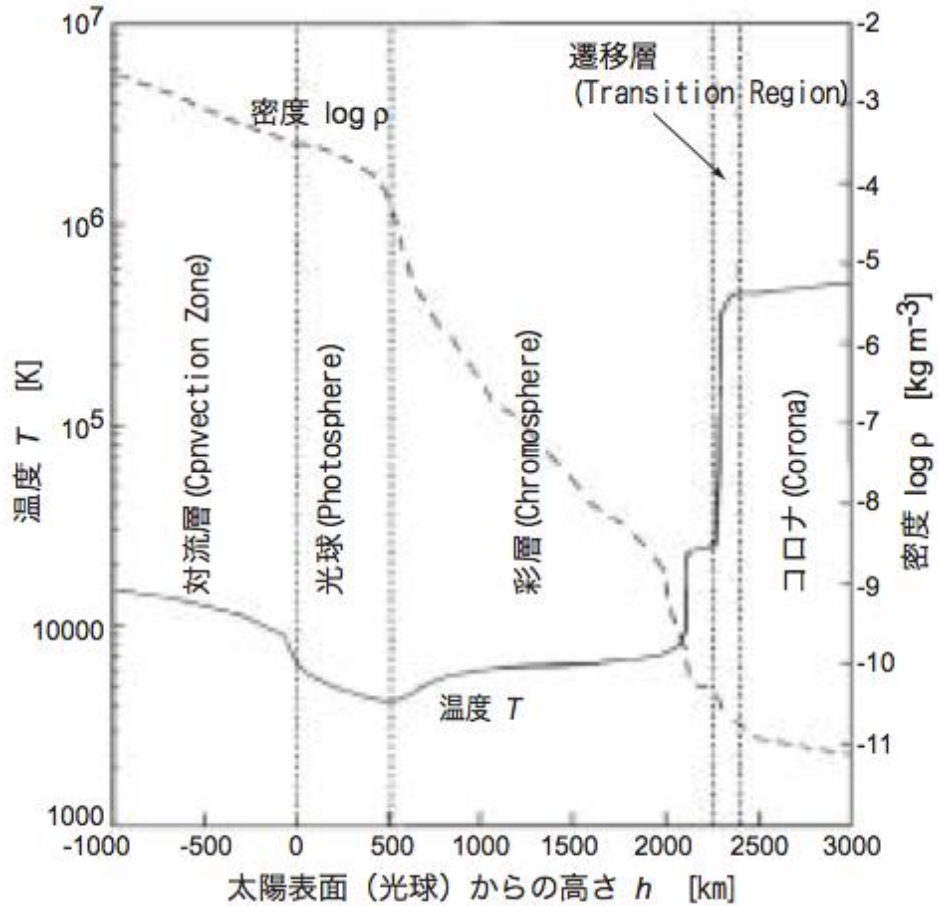


Table 1. Physical parameters and age-rotation relation of well observed and studied solar proxies in comparison with the Sun (after Güdel, 2007).  $L_X$  refers to a range of 0.1–2.4 keV as measured by the ROSAT satellite.

Star name	Type	Mass [ $M_{\text{Sun}}$ ]	Radius [ $R_{\text{Sun}}$ ]	$\log\left(\frac{L_X}{L_{\text{bol}}}\right)$	Rot. [days]	Age [Ga]
HD 129333 [EK Dra]	G1.5 V	1.06	0.95	-3.61	2.68	0.1
HD 72905 [ $\pi^1$ UMa]	G1.5 V	1.03	0.95	-4.47	4.9	0.3
HD 206860 [HN Peg]	G0 V	1.06	0.99	-4.52	4.86	0.3
HD 39587 [ $\chi^1$ Ori]	G1 V	1.01	0.96	-4.65	5.24	0.3
HD 1835 [BE Cet]	G2 V	0.99	1.02	-4.46	7.65	0.6
HD 20630 [ $\kappa^1$ Cet]	G5 V	1.02	0.93	-4.73	9.21	0.65
HD 114710 [ $\beta$ Com]	G0 V	1.08	0.925	-5.52	12	1.6
HD 190406 [15 Sge]	G5 V	1.01	1.1	-5.64	13.5	1.9
Sun	G2 V	1	1	-6.29	25.4	4.6
HD 146233 [18 Sco]	G2 V	1.01	1.03	—	23	4.9
HD 128620 [ $\alpha$ Cen A]	G2 V	1.1	1.22	-6.67	~30	5–6
HD 2151 [ $\beta$ Hyi]	G2 IV	1.1	1.9	-6.41	~28	6.7
HD 186408 [16 Cyg A]	G1.5 V	1	1.16	—	~35	8.5

Table 5. Solar radiation flux enhancement as function of wavelength normalized to the present solar flux value from present to 3.9 Gyr ago (Ribas *et al.*, 2005; Güdel, 2007).

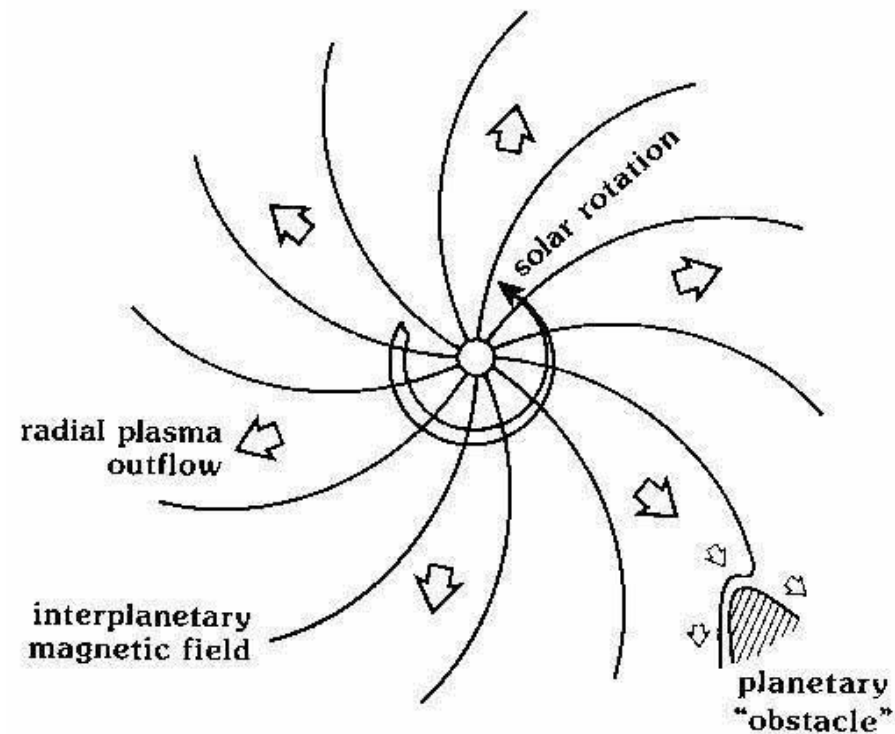
Solar age [Gyr]	$t$ b.p. [Gyr]	X-ray [1–20 Å]	SXR [20–100 Å]	EUV [100–920 Å]	FUV [920–1180 Å]	Lyman- $\alpha$ [1200–1300 Å]	UV [1300–1700 Å]
4.6	0	1	1	1	1	1	1
3.2	1.4	2	1.6	1.5	1.4	1.3	—
2.6	2	3	2	1.9	1.6	1.5	—
1.9	2.7	6	3	2.7	2.1	1.9	2.4
1.1	3.5	16	6	5.1	3.4	2.8	—
0.7	3.9	37	11	8.6	5	3.9	—

# Stellar evolution

- UV radiation from the Sun and late-type stars originates in magnetic chromospheric and transition-zone regions which have been heated to temperatures of  $\sim 10^4$ –  $10^5$  K. Magnetic activity driven by the star's rotation is believed to be critical for this heating.
- For stars with masses  $\leq 1.5 M_{\text{Sun}}$  and ages of about a few 100 Myr, angular momentum loss by a stellar wind brakes rotation. The rotation period of the young Sun was much faster ( $\sim$ few days) during the first 500 Myr after the arrival at the main sequence.
- The radiation and plasma history of our Sun can be separated into a period of a moderate decrease from about 4 Gyr ago to the present and a very early extreme period of about 500 Myr after the young Sun arrived at the main sequence.



**SOLAR WIND**



# 恒星の活動度の変遷

- 恒星のX線、EUV、太陽風、CMEの活動度は、時間とともに自転が遅くなるのに伴つ低下
- 太陽型星の活動度は1億年にわたって高く維持されたと急激に低下
- 質量の小さなM型星では、より長期にわたって高い活動度を維持

Selsis et al. (2007)

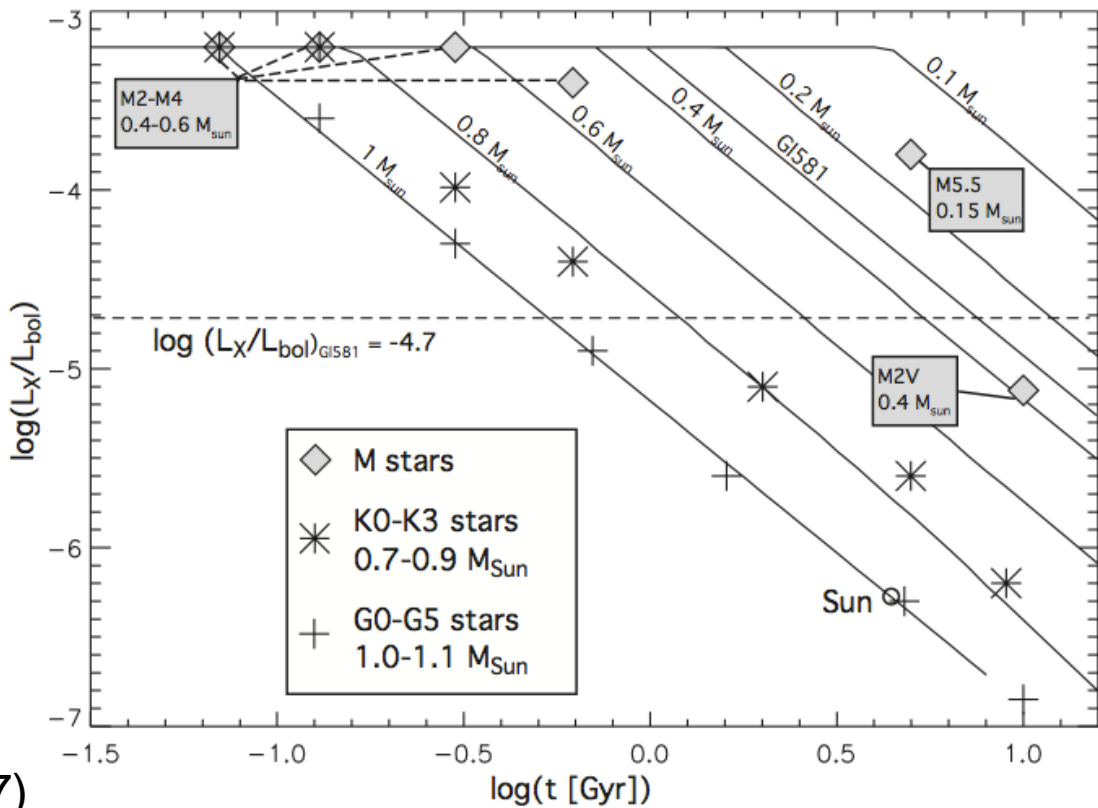


**Fig. 5.** Evolution of the ratio between the X-ray and bolometric luminosities as a function of age for stars of different masses. The solid lines represent semi-empirical laws, while symbols give observed values for G (+), K (\*) and M (◊) stars. The dashed line gives the upper limit for the value of  $\log(L_X/L_{\text{bol}})$  in the case of Gl 581, for which there is no ROSAT detection.

# EUV強度の変化に対する地球熱圏の応答

Tian et al. (2008)

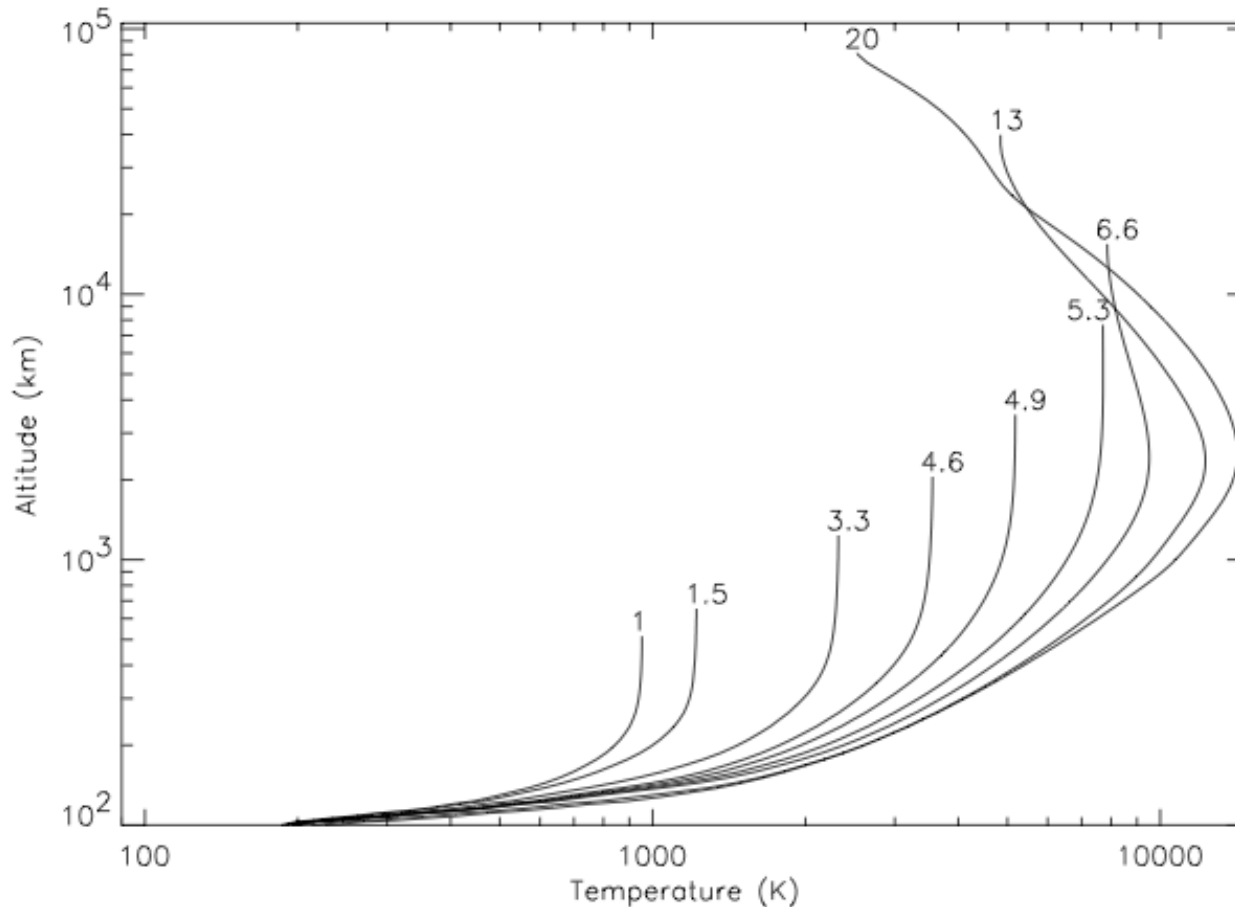
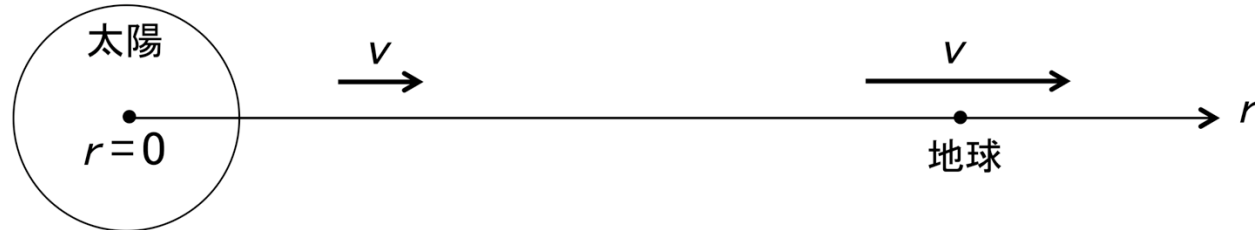


**Figure 6.** Temperature profiles for different solar EUV flux cases (normalized to present-day solar mean energy flux  $\sim 1$  times present EUV, which represents solar EUV energy flux  $\sim 5.1 \text{ mW/m}^2$ ). It is shown that when solar EUV energy flux exceeds certain critical value, the upper part of the thermosphere begins to cool as a result of the increasingly significant adiabatic cooling effect. Beyond the critical flux ( $\sim 5$  times present EUV in this plot), the higher the energy input into the thermosphere, the lower the exobase temperature. This behavior is typical in the studies of hydrodynamic flow in planetary atmospheres.

# A simple solution of hydrodynamic escape

Solar wind is accelerated from subsonic near the Sun to supersonic near the Earth.



Letting the pressure be  $p$ , the mass density be  $\rho$ , the velocity be  $v$ , the gravity constant be  $G$ , and the Solar mass be , we have

$$\frac{1}{r} \frac{dp}{dr} + v \frac{dv}{dr} + \frac{GM}{r^2} = 0$$

$$4\rho r^2 v = \text{const.}$$

$$p = rRT$$



Assuming that the temperature  $T$  does not depend on the distance  $r$ ,

$$\frac{1}{\nu} \frac{\ddot{v}^2}{c_s^2} - \frac{1}{r} \frac{d^2 v}{dr^2} = \frac{2}{r} - \frac{GM}{c_s^2 r^2} \quad c_s = RT : \text{Sound speed}$$

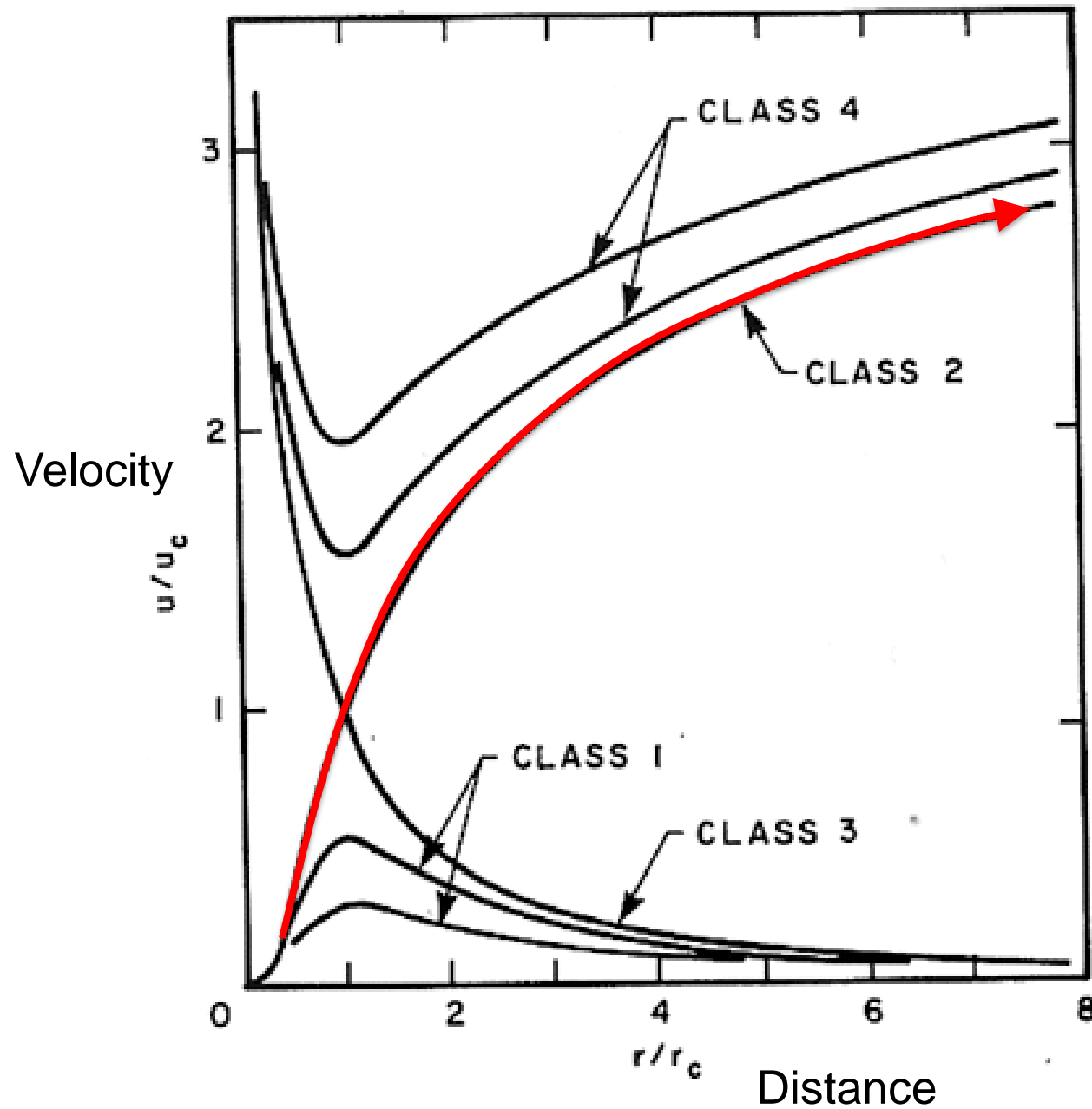
At the point where  $v = c_s$ ,  $dv/dr$  goes to infinity unless the RHS becomes zero there. Therefore, we assume the RHS becomes zero at  $r = r_c$  where  $v = c_s$ . Then we have

$$r_c = \frac{GM}{2c_s^2}$$

In this case,  $dv/dr > 0$  is satisfied both at  $r < r_c$  and  $r > r_c$ , enabling the velocity to be accelerated from subsonic to supersonic.

In the solar wind, letting  $T = 10^6$  K, the velocity exceeds the sound speed at  $r_c = 8 \times 10^6$  km (5% of the Sun-Earth distance).

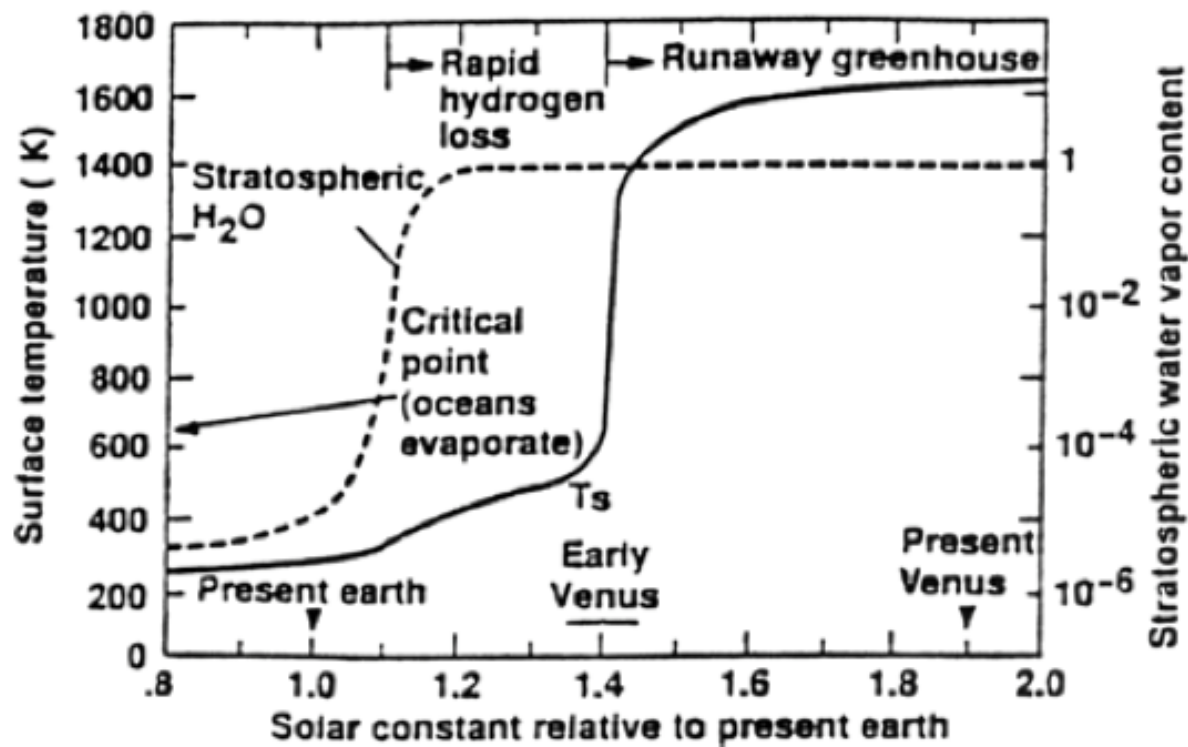
# Solutions of hydrodynamic escape



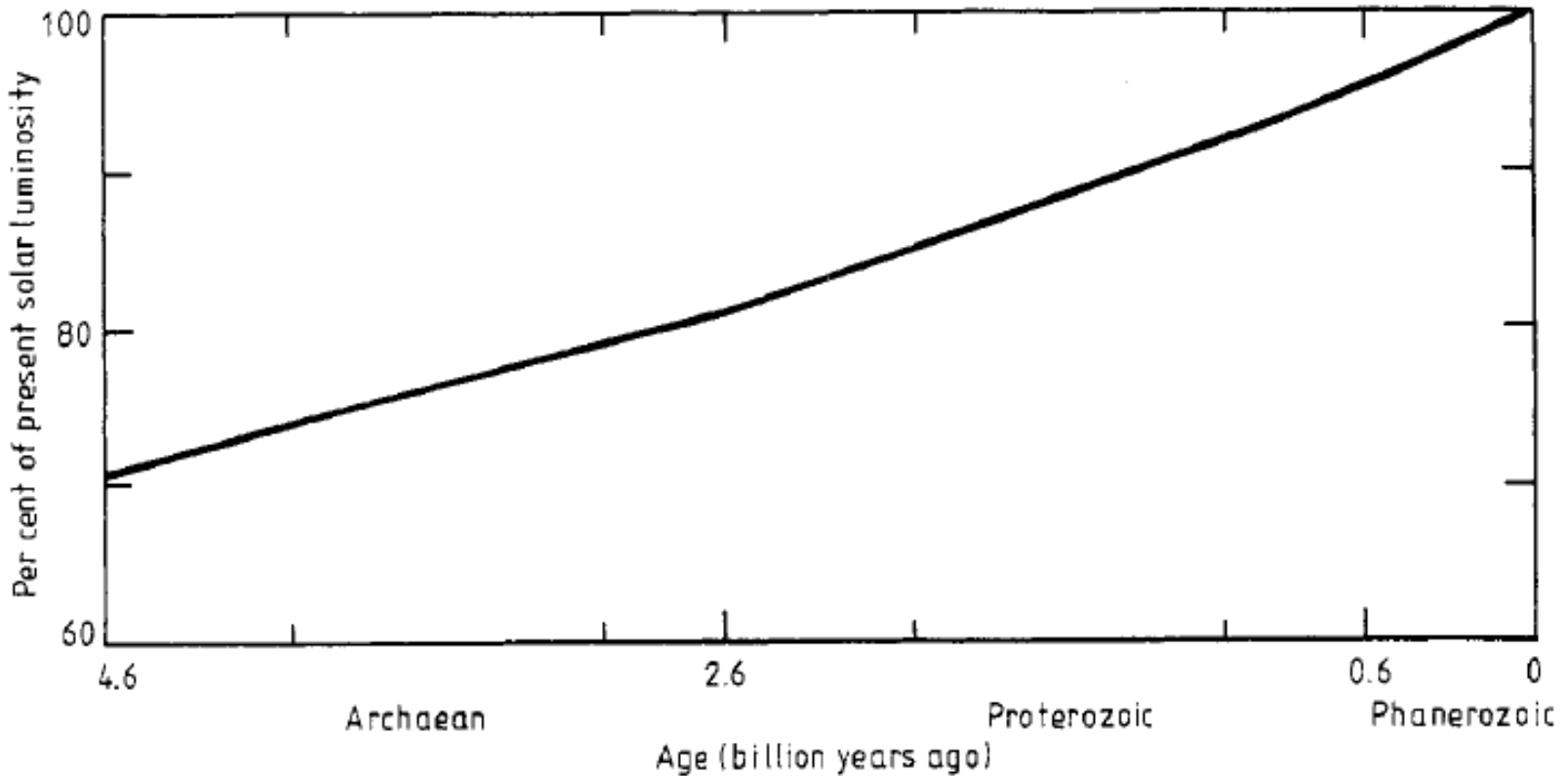
# 金星からの水素の流体的散逸

- かつて金星表面に大量の水があったとしたら、大気中に水蒸気が多く含まれたはず。
- 熱圏下端での水蒸気混合比が増えると熱圏の組成の多くを水素が占めるようになり、分子量の小さな水素はhydrodynamic escapeに至る。

**Fig. 1** Diagram illustrating what would happen to Earth if it were slowly pushed inwards towards the Sun. The *horizontal scale* is the solar flux relative to its value at 1 AU. The *solid curve* represents mean global surface temperature (*left-hand scale*). The *dashed curve* represents stratospheric H<sub>2</sub>O mixing ratio (*right-hand scale*). The solar flux at Venus today and at 4.5 billion years ago is indicated (adapted from Kasting 1988)



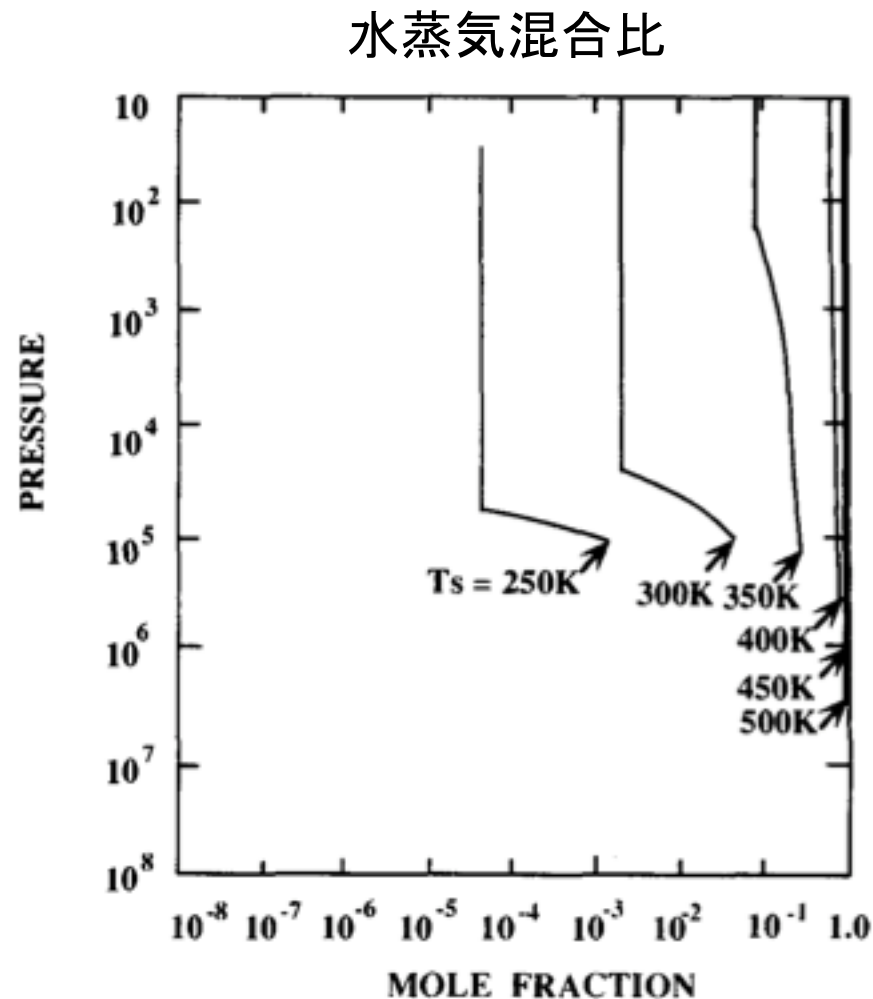
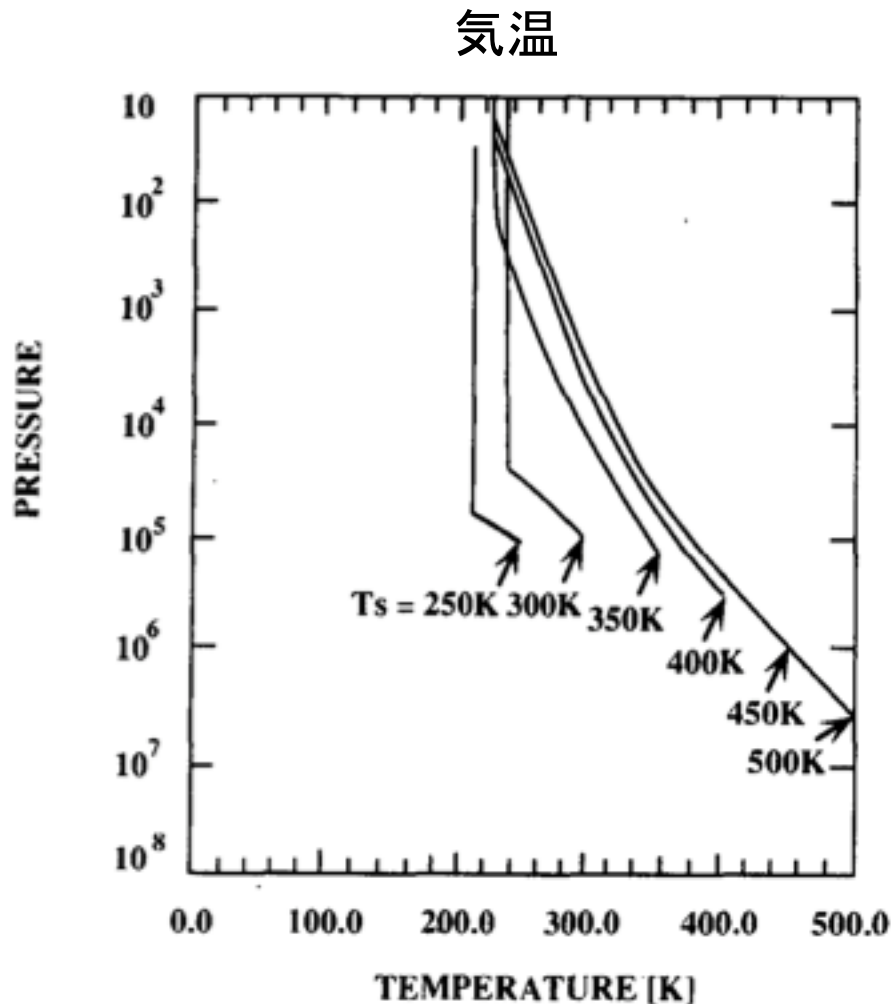
# Long-term trend of solar luminosity



- 標準太陽モデルによれば、太陽は誕生から現在に至るまで、核融合反応により中心部の温度と圧力が上昇する結果として明るさを25～30%増してきた。

# 鉛直1次元モデルによる、海面温度を変えたときの地 球大気の構造変化

Nakajima et al. (1992)



ESCAPE RATES FOR HIGH H<sub>2</sub>O LEVELS

Case	$c_0(\text{H}_2\text{O})$	$\Phi_{\text{esc}}(\text{H})$ (cm <sup>-2</sup> sec <sup>-1</sup> )	$F$ (g ster <sup>-1</sup> sec <sup>-1</sup> )
A	$7.2 \times 10^{-4}$	$2.2 \times 10^9$	$1.3 \times 10^3$
B	$6.3 \times 10^{-3}$	$3.8 \times 10^{10}$	$2.3 \times 10^4$
C	$5.5 \times 10^{-2}$	$1.3 \times 10^{11}$	$7.7 \times 10^4$
D	$4.6 \times 10^{-1}$	$2.7 \times 10^{11}$	$1.6 \times 10^5$

cold trap(高度  
90km、170K)  
での水蒸気混  
合比

計算された  
H流出flux

計算された  
質量流出  
flux

→20億年で地球の  
海と同量が逃げる

昔の太陽紫外線が  
もっと強ければ散逸  
はもっと速くなる

H流出  $1 \times 10^{12} \text{ cm}^{-2} \text{ s}^{-1} \rightarrow$  6億年で地球の海と同量が逃げる  
 $1 \times 10^{11} \text{ cm}^{-2} \text{ s}^{-1} \rightarrow$  60億年で地球の海と同量が逃げる

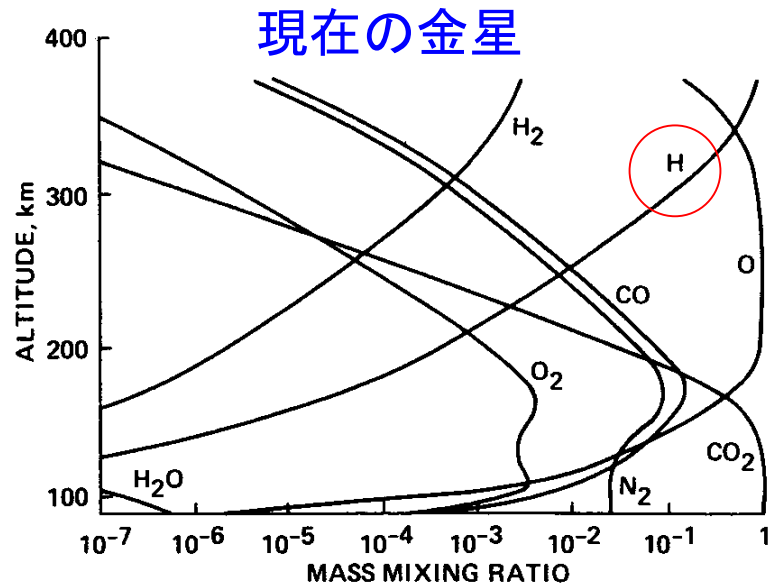


FIG. 2. Mass mixing profiles for the present Venus atmosphere.

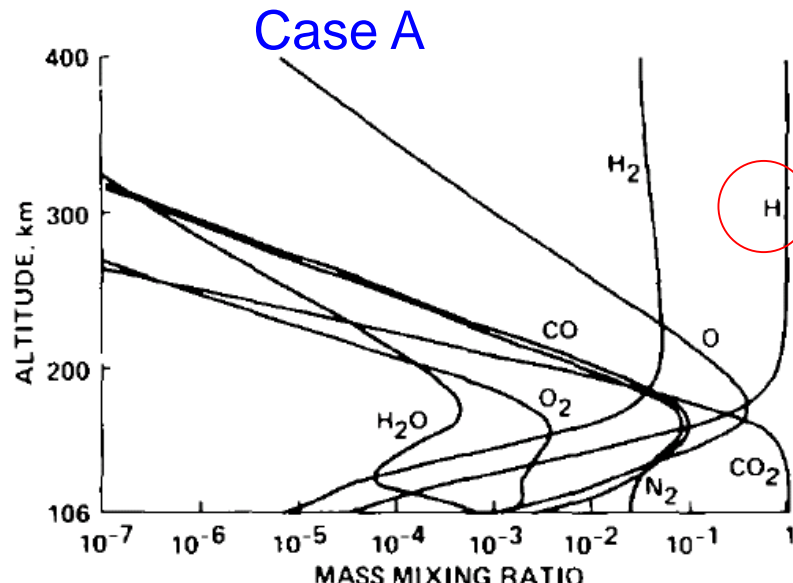


FIG. 9. Mass mixing ratio profiles for Case A.

## 大気組成の高度分布

- 下端の水蒸気混合比が増えると上層大気はほとんどH原子で占められるようになる。
- H原子による紫外線吸収が上層大気の主たる熱源

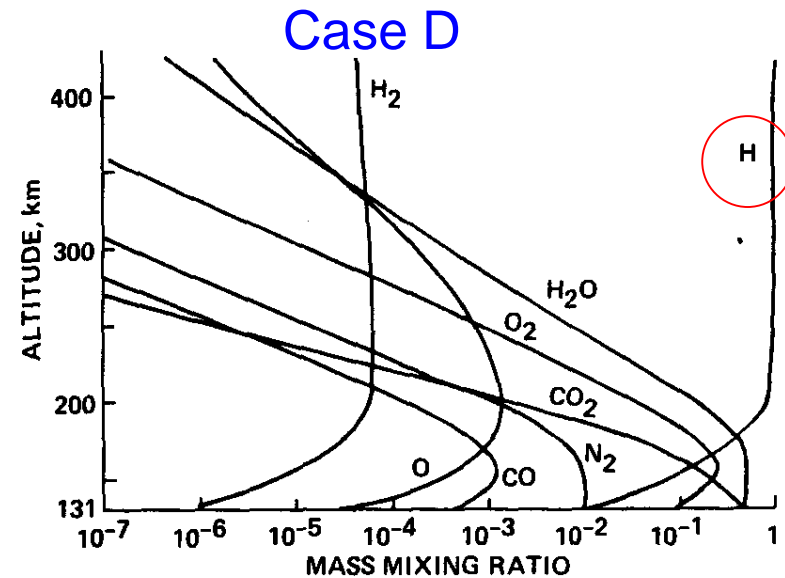


FIG. 10. Mass mixing ratio profiles for Case D.

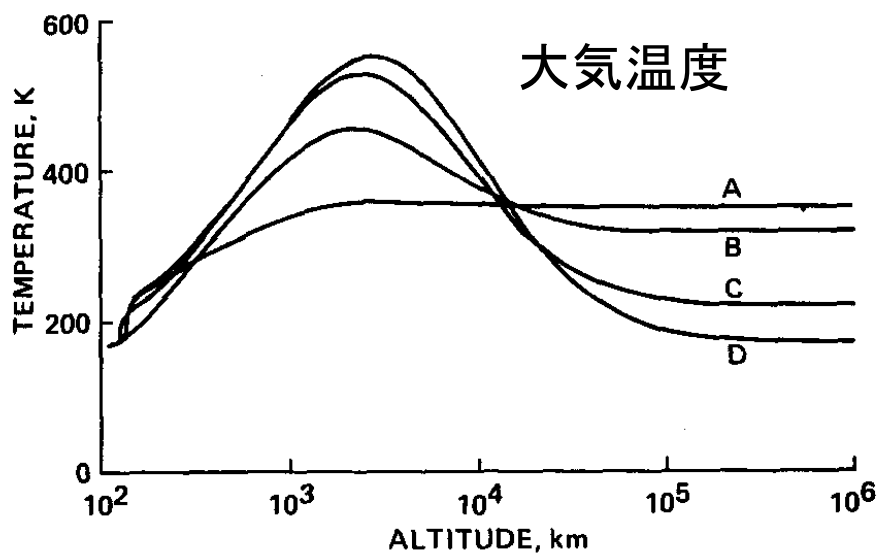


FIG. 5. Temperature profiles for Cases A to D.

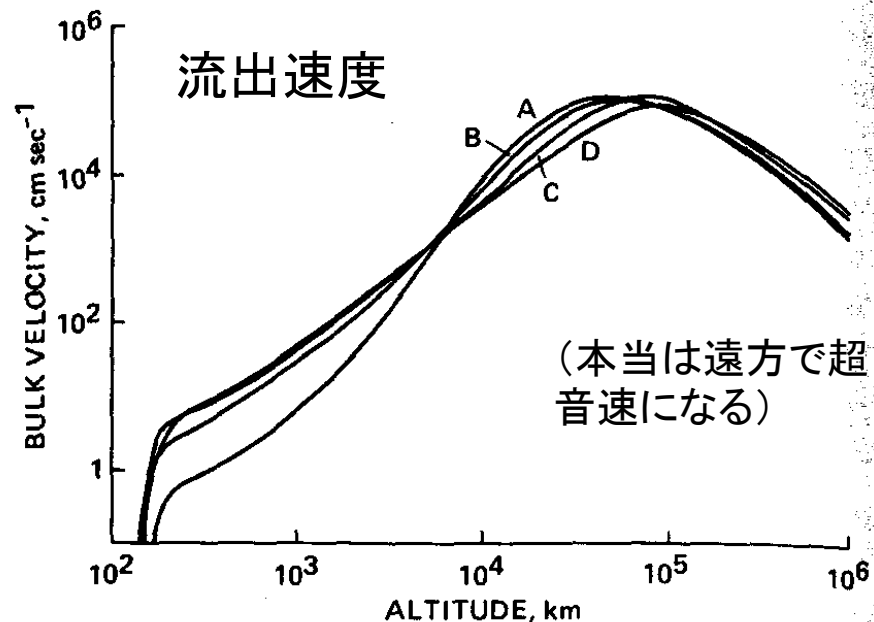


FIG. 6. Bulk velocity profiles for Cases A to D.  
(本当は遠方で超音速になる)

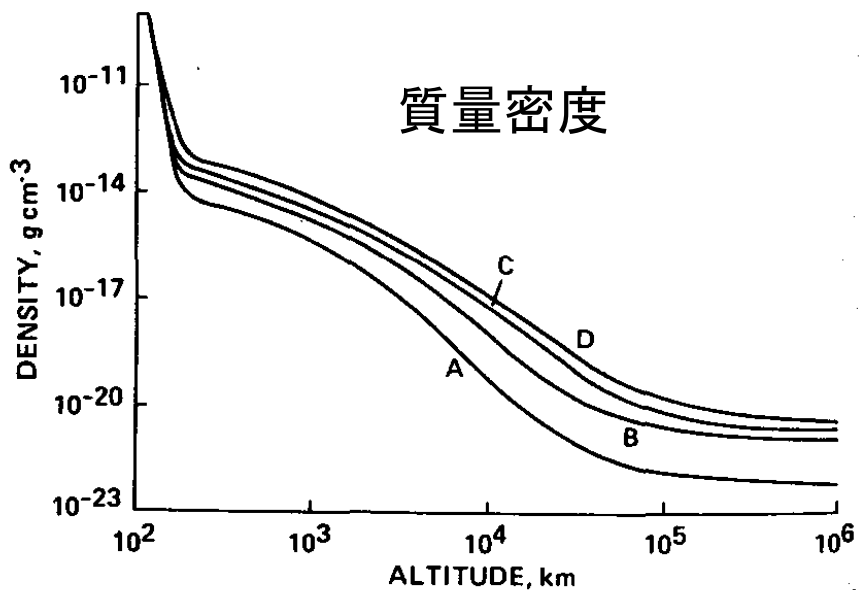


FIG. 7. Mass density profiles for Cases A to D.

- Terrestrial planets may evolve through phases where their upper atmospheres are hydrogen-rich.
- High  $c_{\text{H}_2\text{O}}$  ( $\text{H}_2\text{O}$  mixing ratio) levels and/or high XUV fluxes result in  $\Phi_{\text{H}}$  (escape flux) in the range of about  $10^{11}\text{--}10^{13} \text{ cm}^{-2} \text{ s}^{-1}$ .

Table 4

Escape fluxes of atomic hydrogen during hydrodynamic conditions from Venus' upper atmosphere as a function of various mesopause  $\text{H}_2\text{O}$  mixing ratios  $c_{\text{H}_2\text{O}}$  and solar XUV flux (see Kasting and Pollack, 1983)

$c_{\text{H}_2\text{O}}$	0.00072	0.0063	0.055	0.46
XUV flux $\phi_{\text{H}}$ ( $\text{cm}^{-2} \text{ s}^{-1}$ )				
1	$\sim 2.2 \times 10^9$	$\sim 3.8 \times 10^{10}$	$\sim 1.3 \times 10^{11}$	$\sim 2.7 \times 10^{11}$
2	$\sim 6.5 \times 10^9$	$\sim 9.3 \times 10^{10}$	$\sim 3.2 \times 10^{11}$	$\sim 6.6 \times 10^{11}$
4	$\sim 1.0 \times 10^{10}$	$\sim 1.8 \times 10^{11}$	$\sim 6.2 \times 10^{11}$	$\sim 1.3 \times 10^{12}$
8	$\sim 1.8 \times 10^{10}$	$\sim 3.2 \times 10^{11}$	$\sim 1.0 \times 10^{12}$	$\sim 2.3 \times 10^{12}$
16	$\sim 2.8 \times 10^{10}$	$\sim 4.9 \times 10^{11}$	$\sim 1.7 \times 10^{12}$	$\sim 3.5 \times 10^{12}$
100	$\sim 2.2 \times 10^{11}$	$\sim 3.8 \times 10^{12}$	$\sim 1.3 \times 10^{13}$	$\sim 2.7 \times 10^{13}$

Kulikov et al. (2006)

しかし水素は逃げても酸素が逃げるのは容易でない

# 微惑星の衝突脱ガスで生じる初期地球の大気の組成

## Hashimoto et al. (2007)

もとはかなり還元的だった可能性も

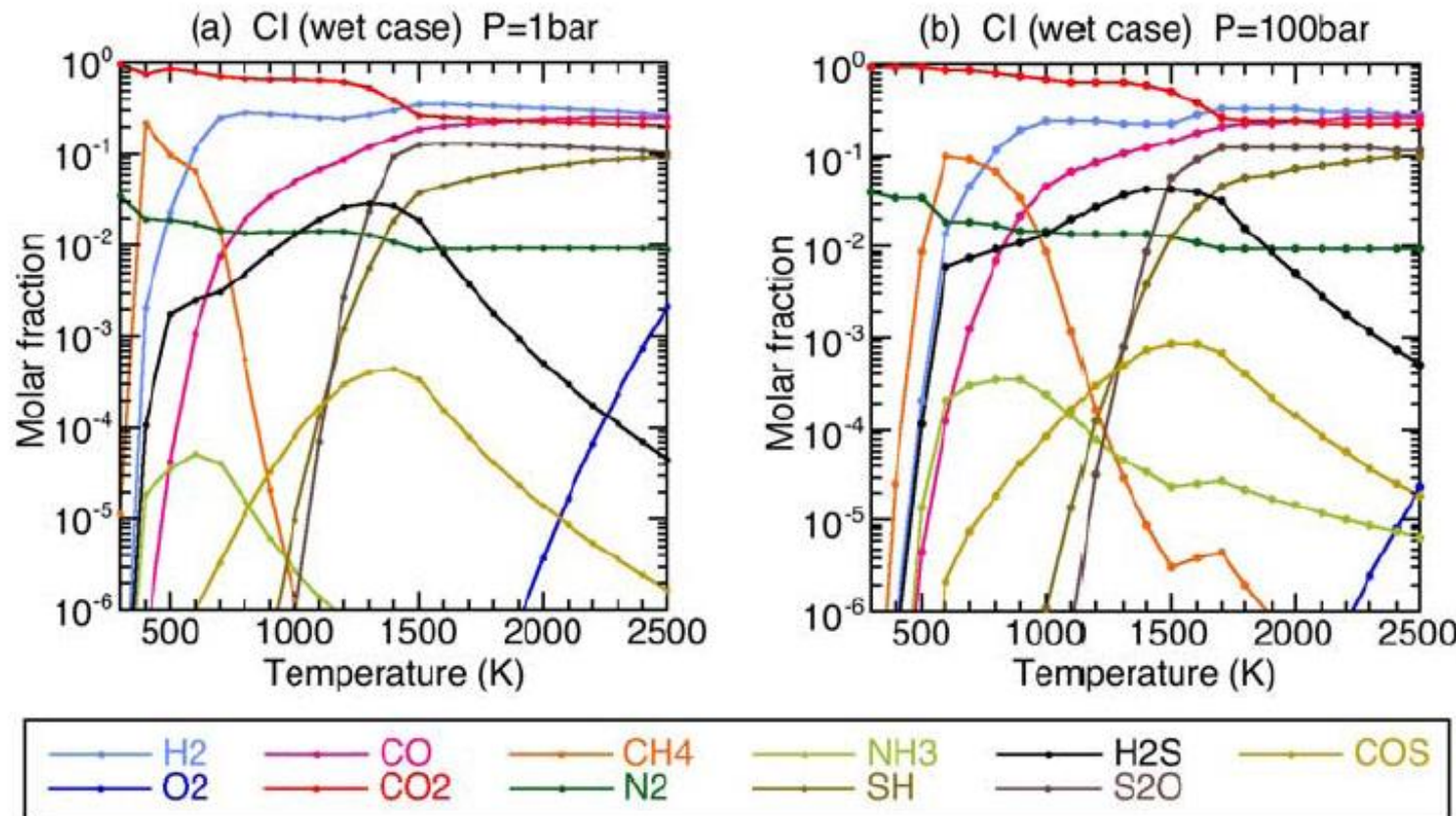
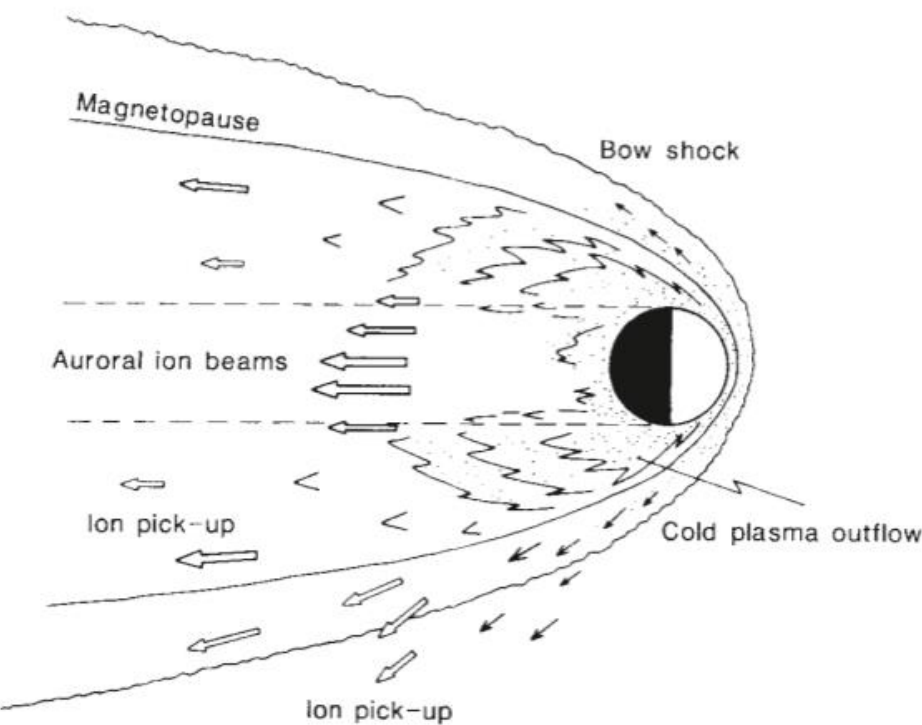


**Figure 1.** Equilibrium composition of dry gas phase at (a) 1 bar and (b) 100 bar total pressures. Water content in CI chondrite is about 20 wt% (wet case). This figure does not include water vapor since atmospheric water varies greatly due to condensation.

# 火星からの非熱的散逸

- Phobos探査機により現在の火星からの大気散逸を観測
- 酸素の散逸量は、現在の火星大気のCO<sub>2</sub>に含まれる酸素を1億年で失わせる程度。あるいは、45億年で深さ1mの海に含まれる酸素を失わせる程度。



Lundin et al. (1989)

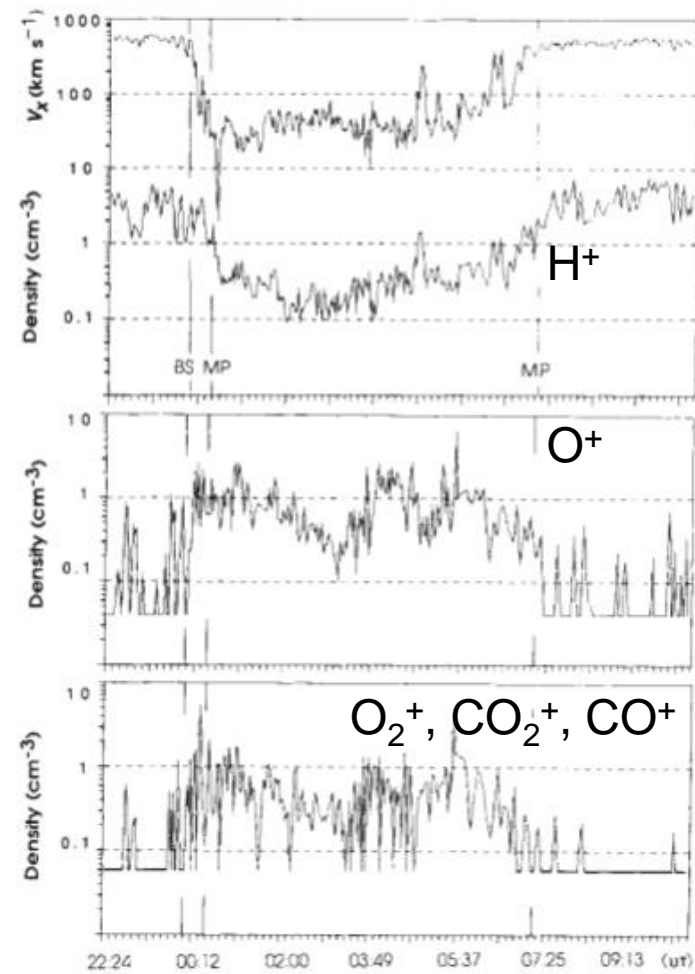


FIG. 2 Moment parameters for O<sup>+</sup> and H<sup>+</sup> ions during the second Phobos 2 orbit around Mars (4–5 February 1989). The top panel gives the flow velocity and the number density of H<sup>+</sup> ions. The middle and lower depict the number density of O<sup>+</sup> and molecular ions (O<sub>2</sub><sup>+</sup>, CO<sub>2</sub><sup>+</sup>, CO<sup>+</sup>), respectively. The inbound bow shock (BS) and magnetopause (MP), and the outbound magnetopause crossings are marked by vertical lines.

表3.1：非熱的散逸の例

電荷交換	$H + H^{+*} \rightarrow H^+ + H^*$
	$O + H^{+*} \rightarrow O^+ + H^*$
解離性再結合	$O_2^+ + e \rightarrow O^* + O^*$
	$OH^+ + e \rightarrow O + H^*$
衝突解離	$N_2 + e^* \rightarrow N^* + N^*$
光解離	$O_2 + h\nu \rightarrow O^* + O^*$
イオン-中性粒子反応	$O^+ + H_2 \rightarrow OH^+ + H^*$
スパッタリング/ノックオン	$Na + S^{+*} \rightarrow Na^* + S^+$
太陽風ピックアップ	$O^+ + h\nu \rightarrow O^+ + e$

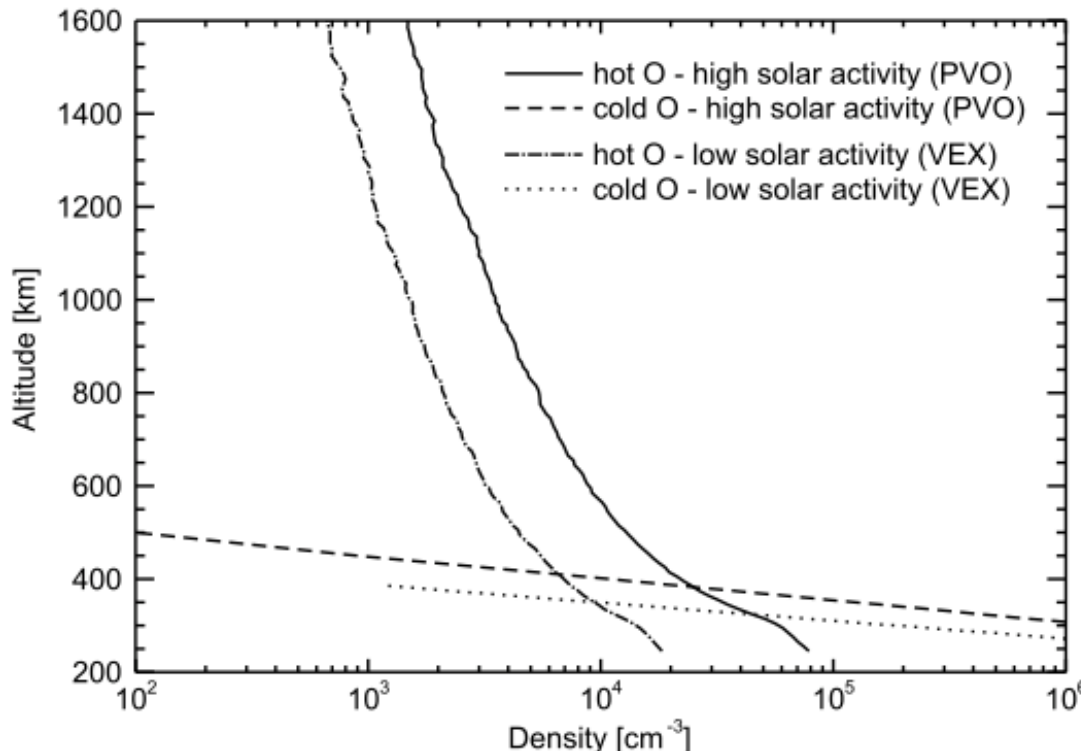
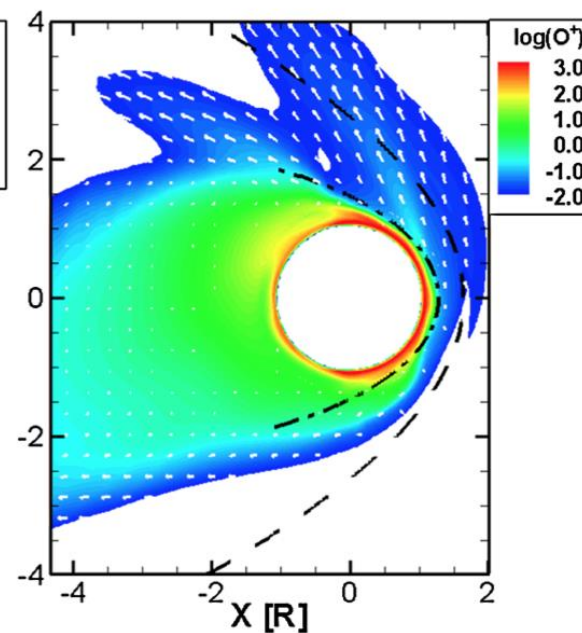
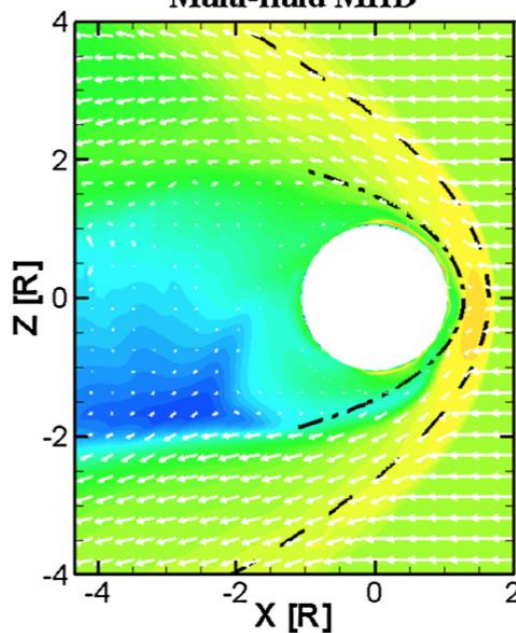


Fig. 9. Photochemically produced supra-thermal “hot” O atom density profiles at present Venus during low and high solar activity conditions compared with the bulk atmosphere.

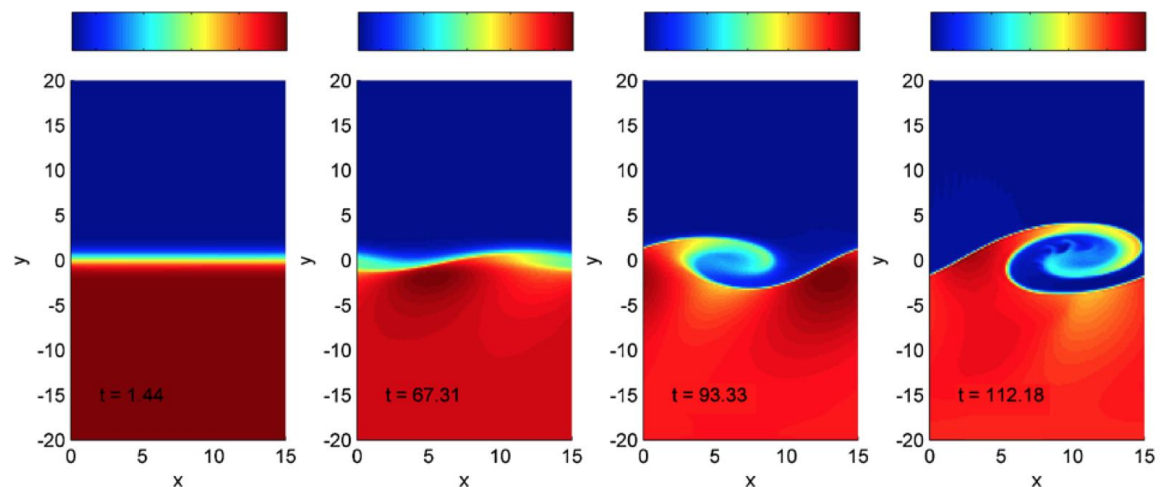
# Bulk plasma escape

Multi-fluid MHD



K-H (shear) instability

Ma et al. 2004, Najib et al. 2011



# Evolution of escape rates

Chassefiere et al. (2007)

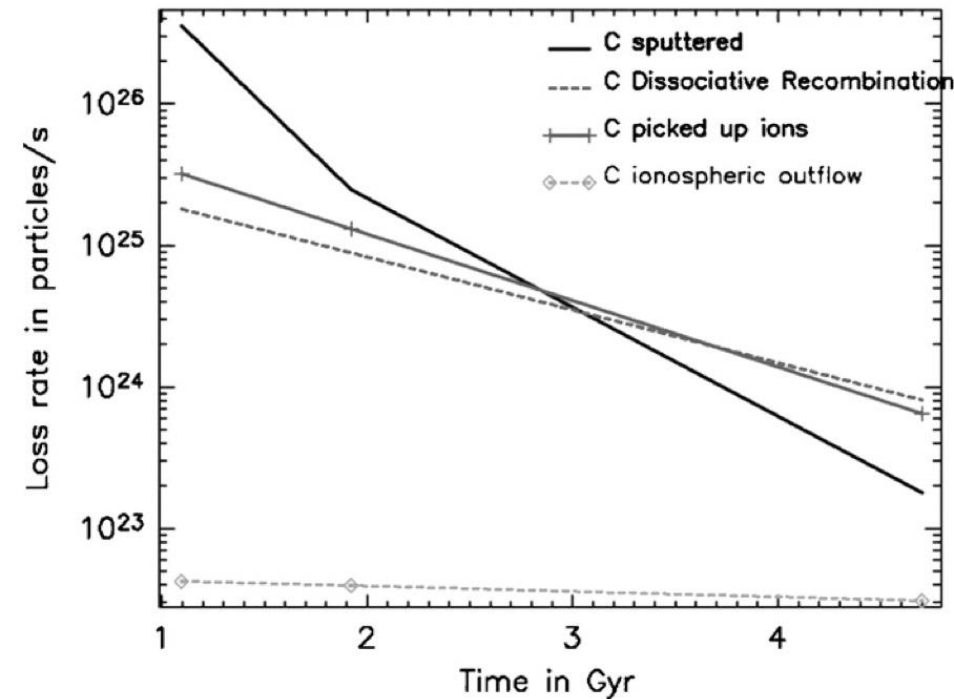
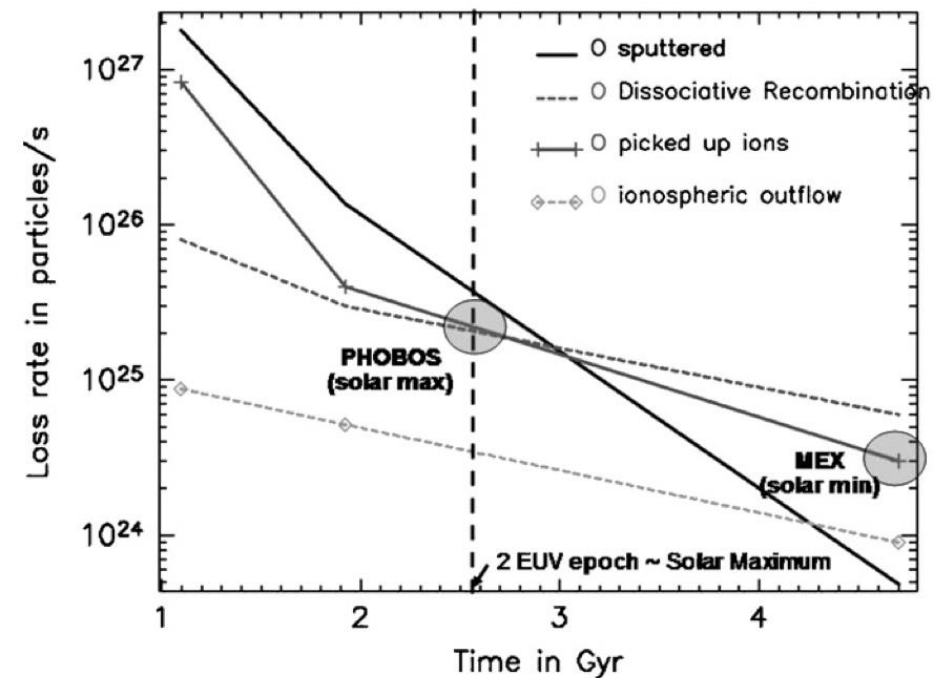
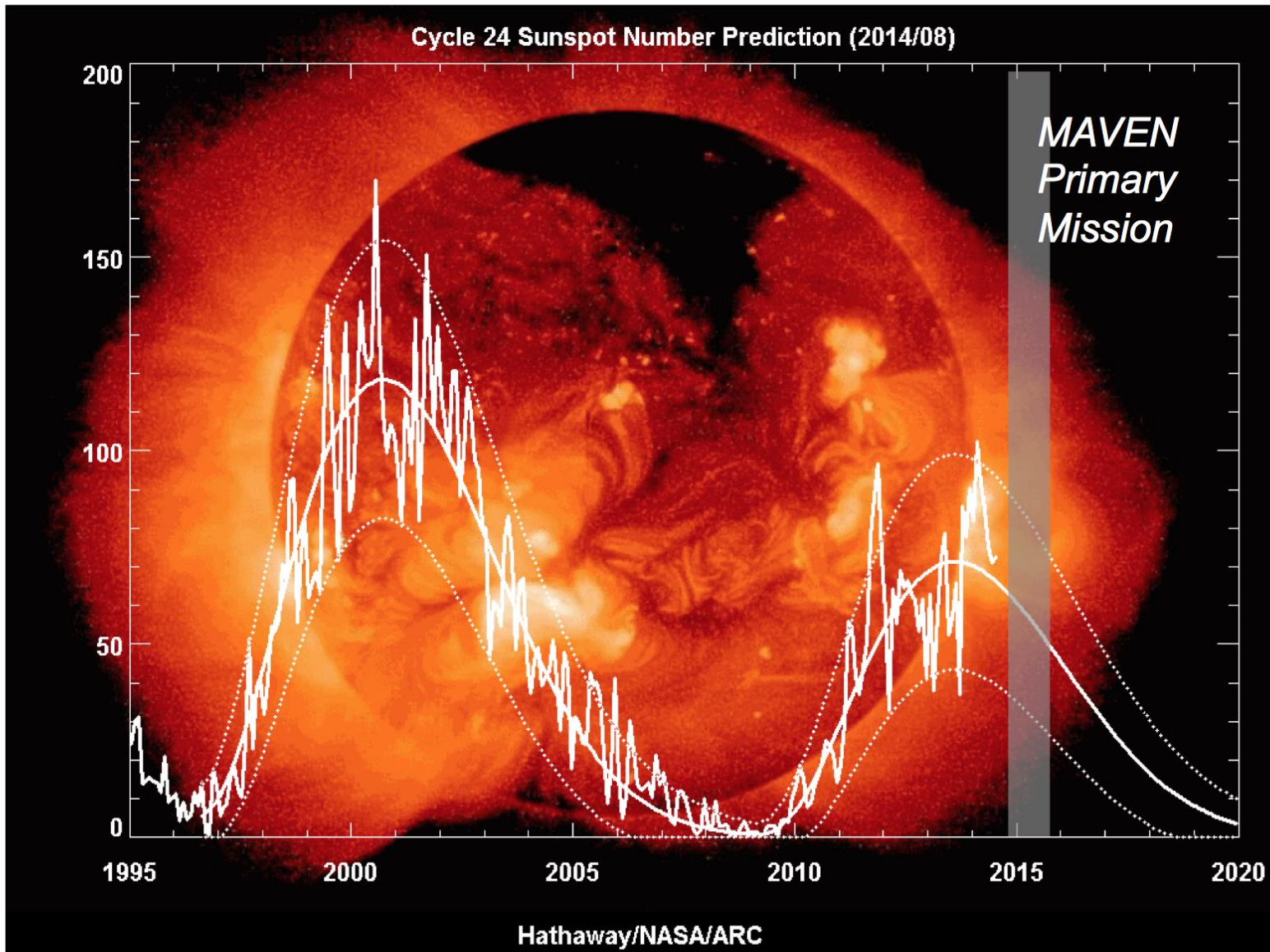


Fig. 4. Evolution of the escape rate of oxygen (upper panel) and of carbon (lower panel) due to non-thermal mechanisms of escape applied to the Martian atmosphere (estimated as described in the text). On the upper panel are also indicated the measured escape rate of total ion oxygen (probably the sum of the ion escape and ionospheric outflow) reported by Lundin et al. (1989) for solar maximum conditions (from ASPERA on Phobos spacecraft) and the escape rate recently estimated from ASPERA electron measurements on board Mars Express for solar minimum conditions (Sauvaud A., personal communication).

# MAVEN's Timing in the Solar Cycle



*MAVEN's primary mission occurs on the declining phase of the solar cycle, when solar storms are most intense and most abundant.*

# Mars Atmosphere and Volatile Evolution (MAVEN) mission

Arrive at Mars : September 21, 2014



# MAVEN Science instruments

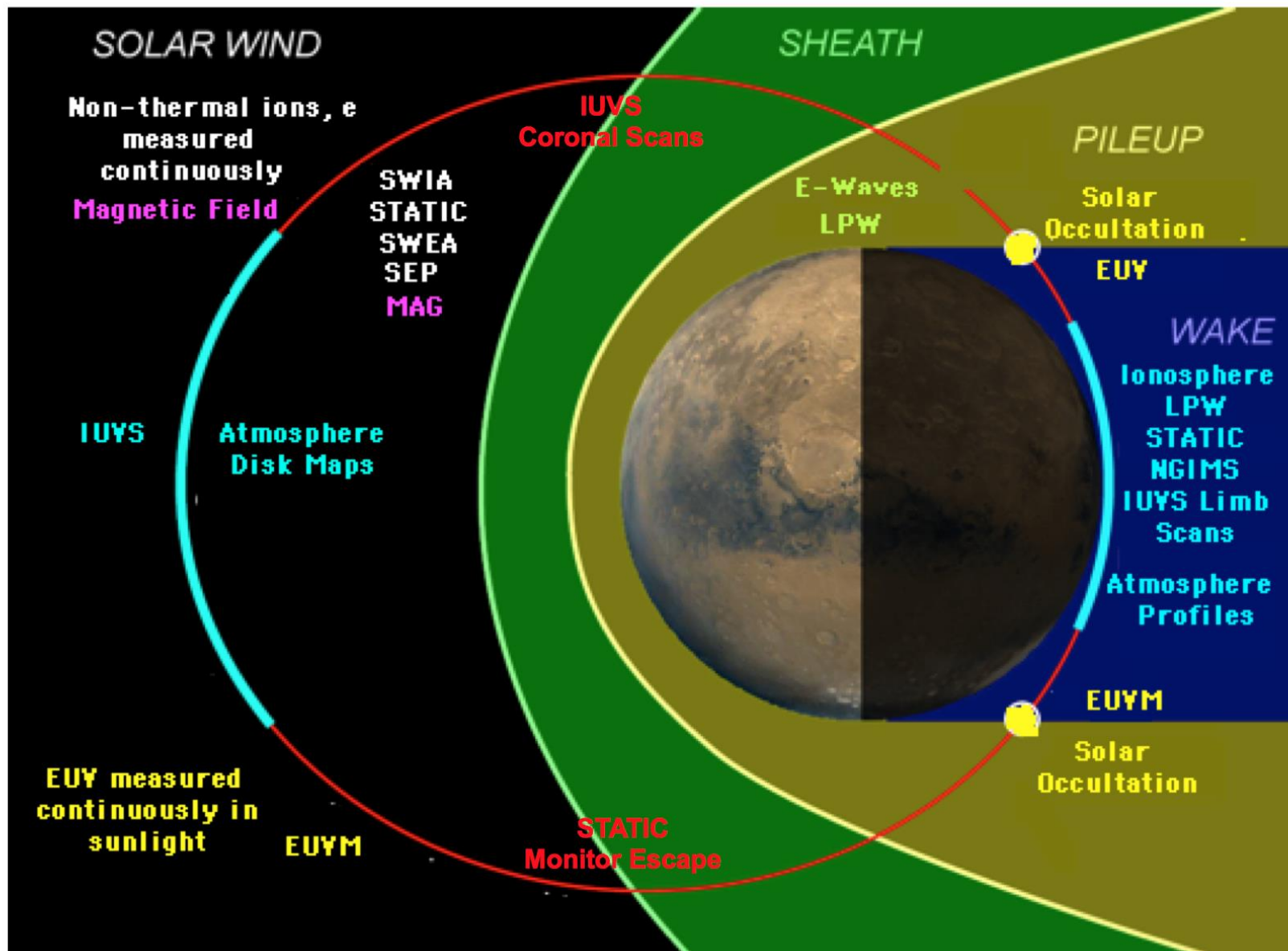
- NGIMS (Neutral Gas and Ion Mass Spectrometer)
  - He, N, O, CO, N<sub>2</sub>, O, O<sub>2</sub>, Ar and CO<sub>2</sub>, and their major isotopes
  - thermal O<sup>+2</sup>, CO<sup>+2</sup>, NO<sup>+</sup>, O<sup>+</sup>, CO<sup>+</sup>, C<sup>+</sup>, N<sup>+2</sup>, OH<sup>+</sup>, and N<sup>+</sup>
- LPW (Langmuir Probe and Waves)
  - thermal electron density and temperatures
  - electric field wave power at frequencies important for ion heating
- STATIC (Supra-thermal and Thermal Ion Composition)
  - major ions (H<sup>+</sup>, O<sup>+</sup>, O<sup>+2</sup>, CO<sup>+2</sup>), their corresponding ion temperatures (~0.02 eV to >10 eV), and the 3-component (X,Y,Z) ion flow velocities (~0.2 to 25 km/s)
- IUVS (Imaging Ultraviolet Spectrometer)
  - H, C, N, O, CO, N<sub>2</sub>, and CO<sub>2</sub>
  - C<sup>+</sup> and CO<sup>+2</sup>
- SEUV (Solar Extreme Ultraviolet)
  - solar irradiance at soft X-ray (0.1–7.0 nm), EUV (17–22 nm), and UV (Lyman- $\alpha$ ) wavelengths
- SEP (Solar Energetic Particle)
  - energy spectrum and angular distribution of solar energetic electrons (30–300 keV) plus protons and heavier ions (30 keV–6 MeV)

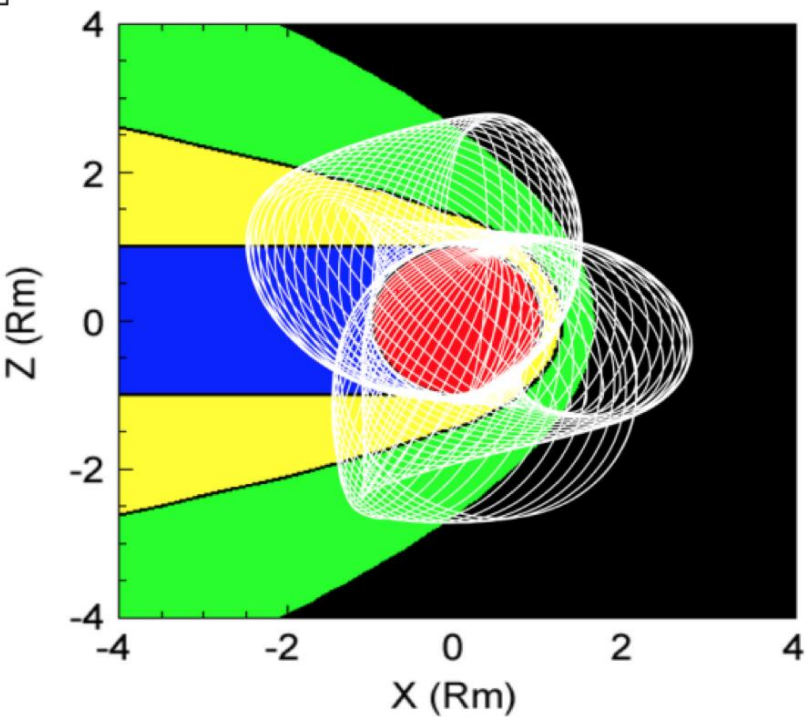
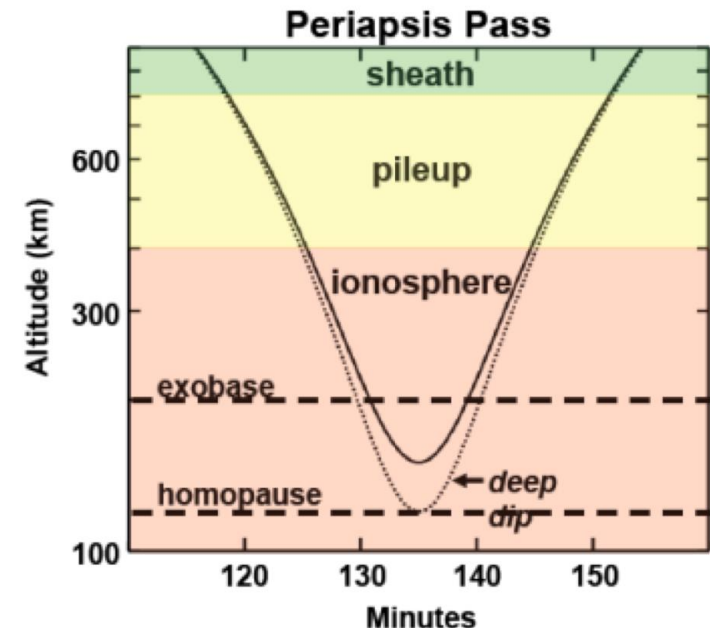
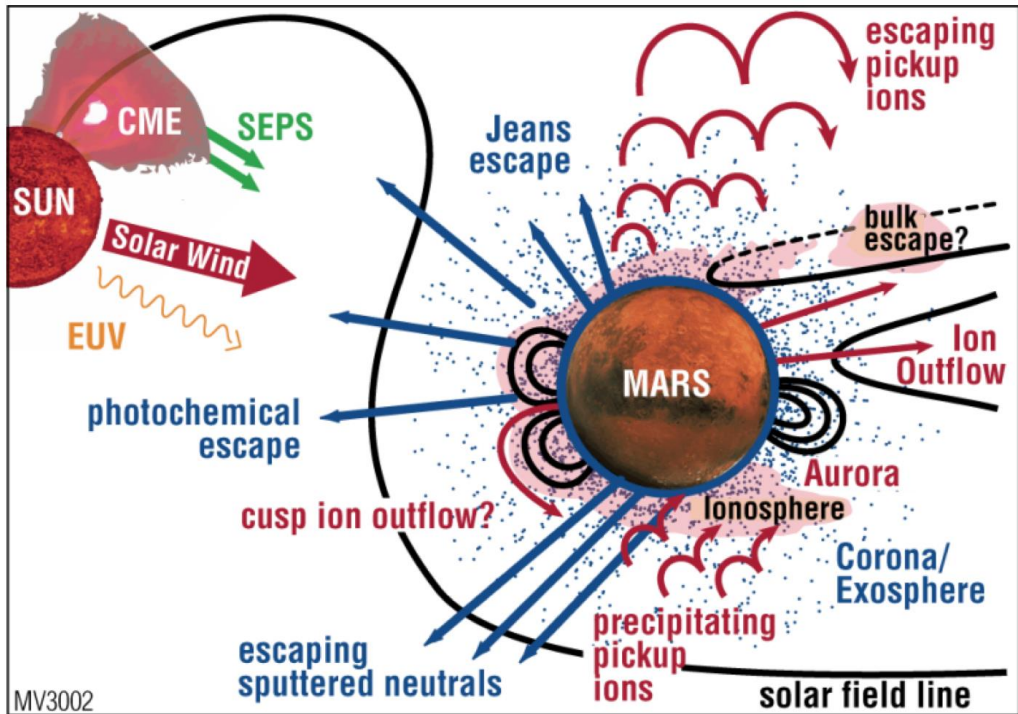
# The MAVEN Spacecraft

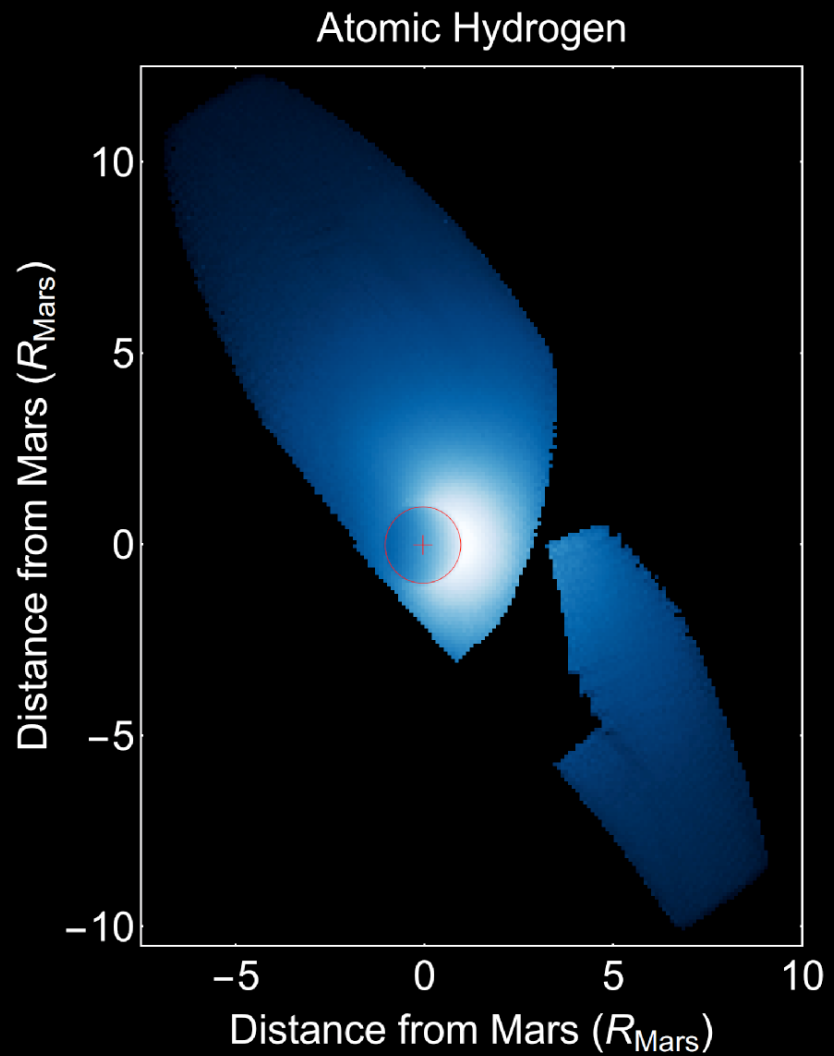
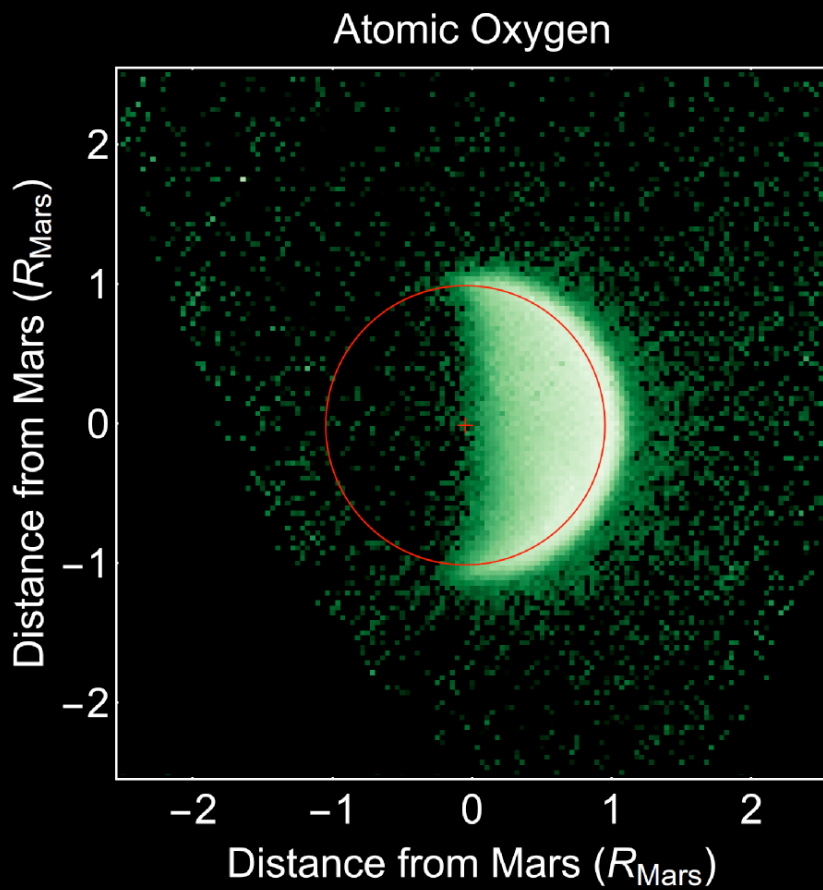
- Launch (Wet) Mass: 2455 kg at launch
- Spacecraft Dry Mass: 810 kg at launch
- Power: 1135 W at Mars Aphelion



# MAVEN Observes All Regions Of Near-Mars Space Throughout The Orbit







# Discovery of diffuse aurora on Mars

## Schneider et al. (2015)

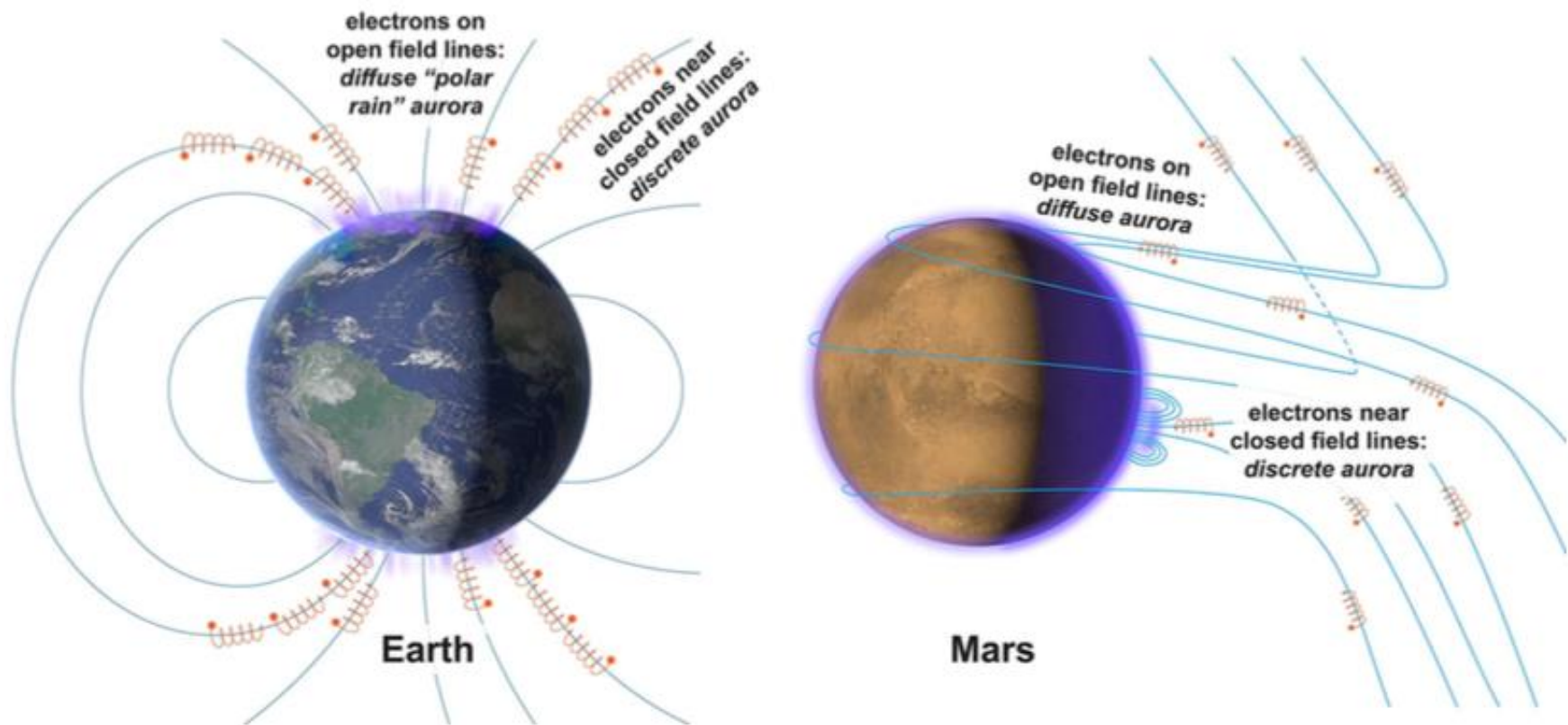
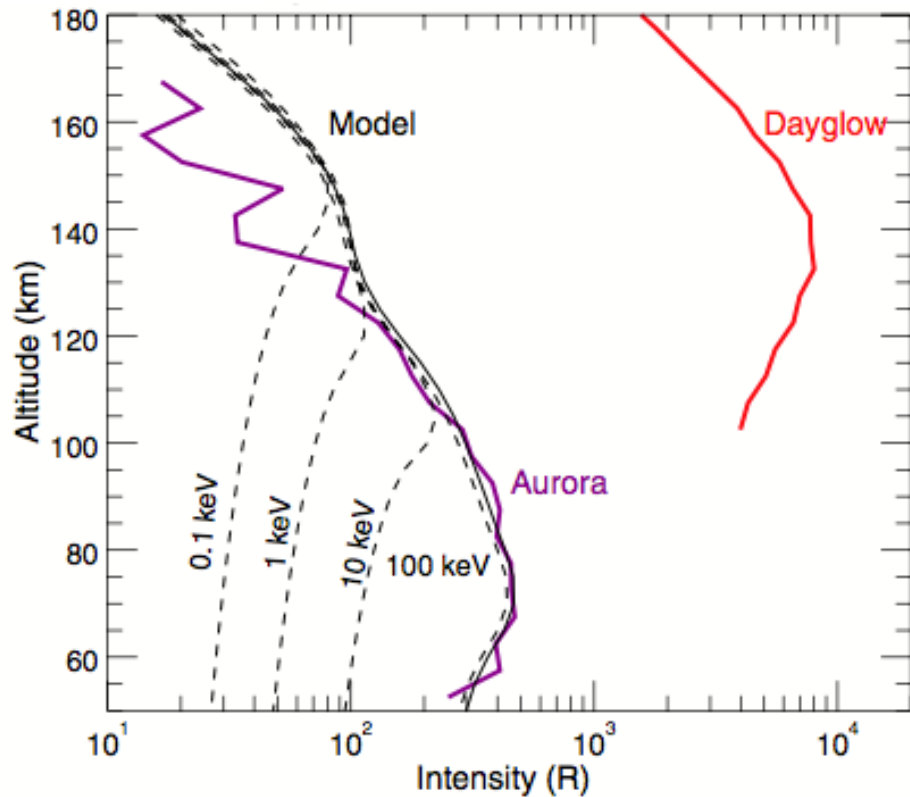
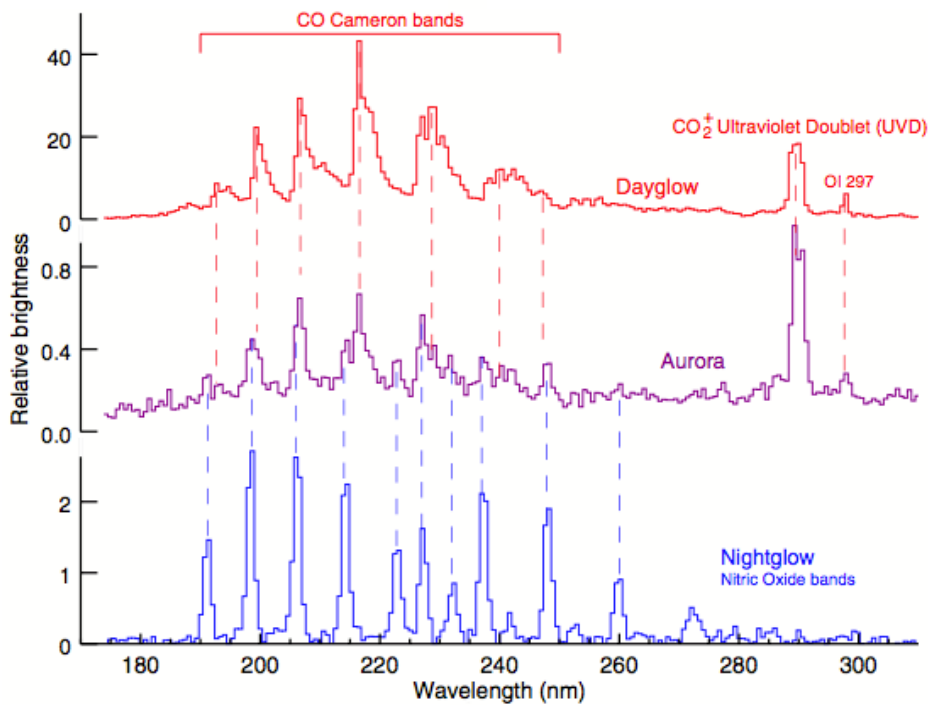


**Fig. 5. Comparison of field geometry for diffuse and discrete auroras on Earth and Mars.** Mars lacks an internally generated global magnetic field, due to the cooling of its core. Fields surrounding Mars are a combination of small structures locked in the crust billions of years ago (lower right) and solar wind field lines draped around the planet.

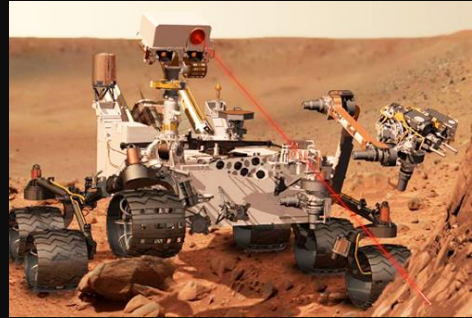


"Diffuse auroras may have additional effects on atmospheric processes. Only a fraction of the deposited energy results in atmospheric excitation and emission. Incident particles also ionize and dissociate atmospheric species, as well as heat the target atmosphere. These effects can lead to increased atmospheric escape rates: Ionized particles at sufficient altitudes can escape via outflow processes, and atmospheric heating can lead to increased thermal escape."

# 火星の気候変動

# 火星の古気候

火星探査車キュリオシティ



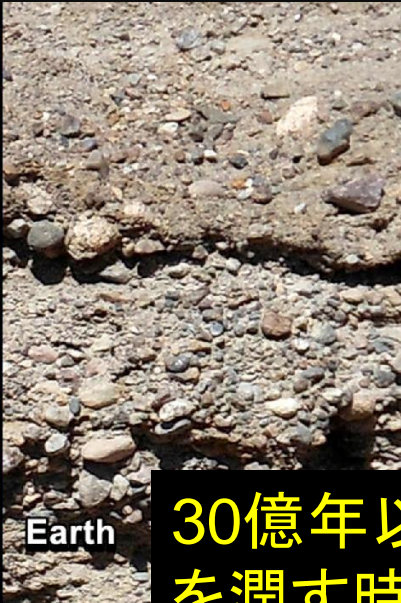
火星の流水地形



火星のたい積岩



地球のたい積岩



30億年以上前にはあたたかくて水が地表を潤す時代があったかもしれない

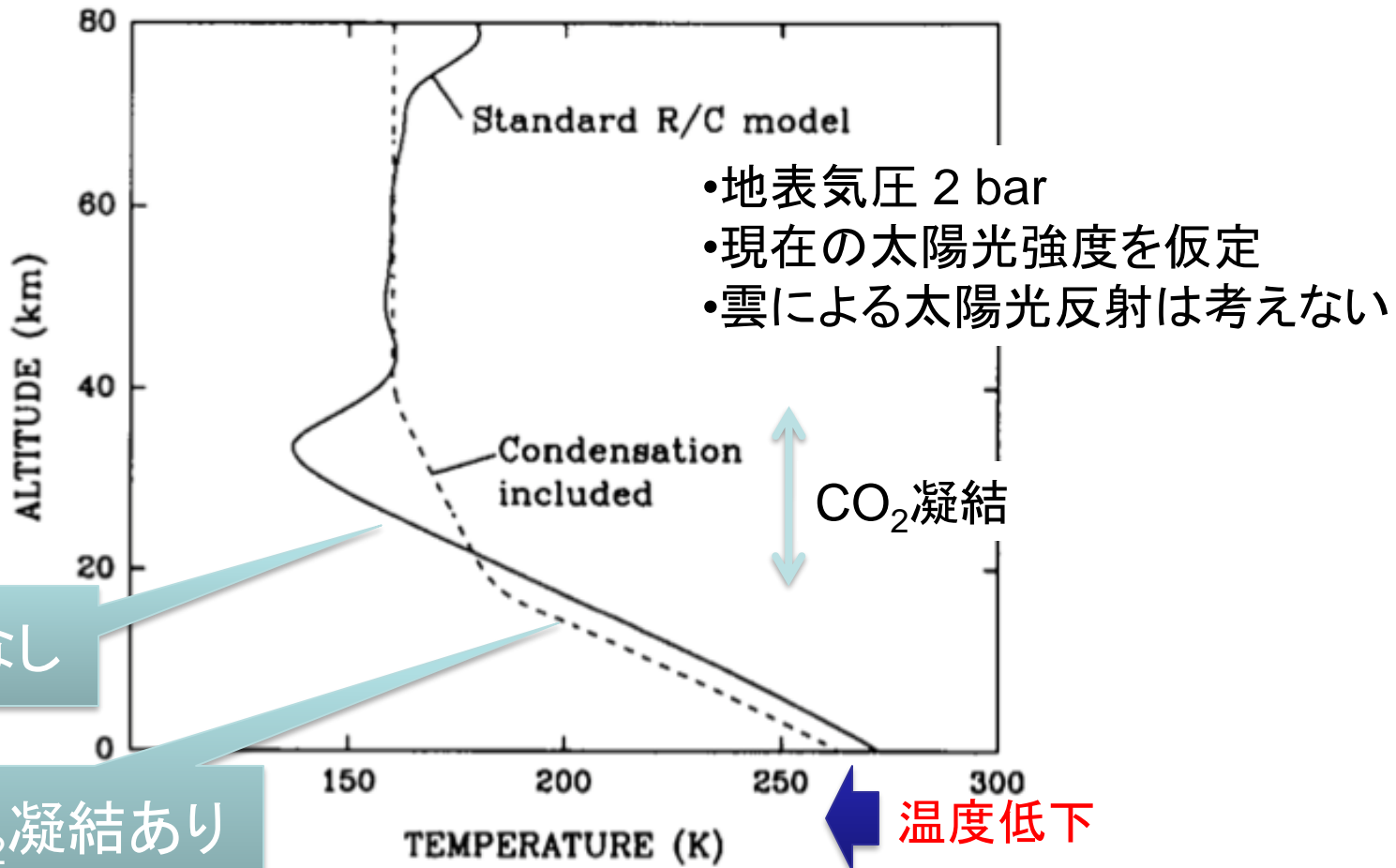
# 初期火星はCO<sub>2</sub>の温室効果で暖まるか

Kasting (Icarus, 1991)

- 太陽光が現在より25%暗い初期の火星環境においても、CO<sub>2</sub>が十分にあれば0°C以上を実現できるか
- 温室効果で地表近くが暖まっても上空は冷たいので、CO<sub>2</sub>が凝結することを考慮する必要がある。
- 温室効果で地表近くの大気が暖められると成層が不安定となり対流が生じる。対流により持ち上げられた空気は断熱膨張で温度が下がり、大気成分が凝結する。凝結熱が大気を暖めるために高度方向の温度低下は小さく抑えられる。
- このことは地表温度にどう影響するか

# $\text{CO}_2$ 凝結の効果

- $\text{CO}_2$ 凝結が起こる領域では温度減率が小さくなる。
- 高高度で温度が上がると、地表 + 大気から宇宙に放射される熱放射フラックスを同じに保つために、低高度の温度は下がる。
- 太陽光強度が現在の86%以下だと厚い $\text{CO}_2$ 大気でも地表温度は0°C以下

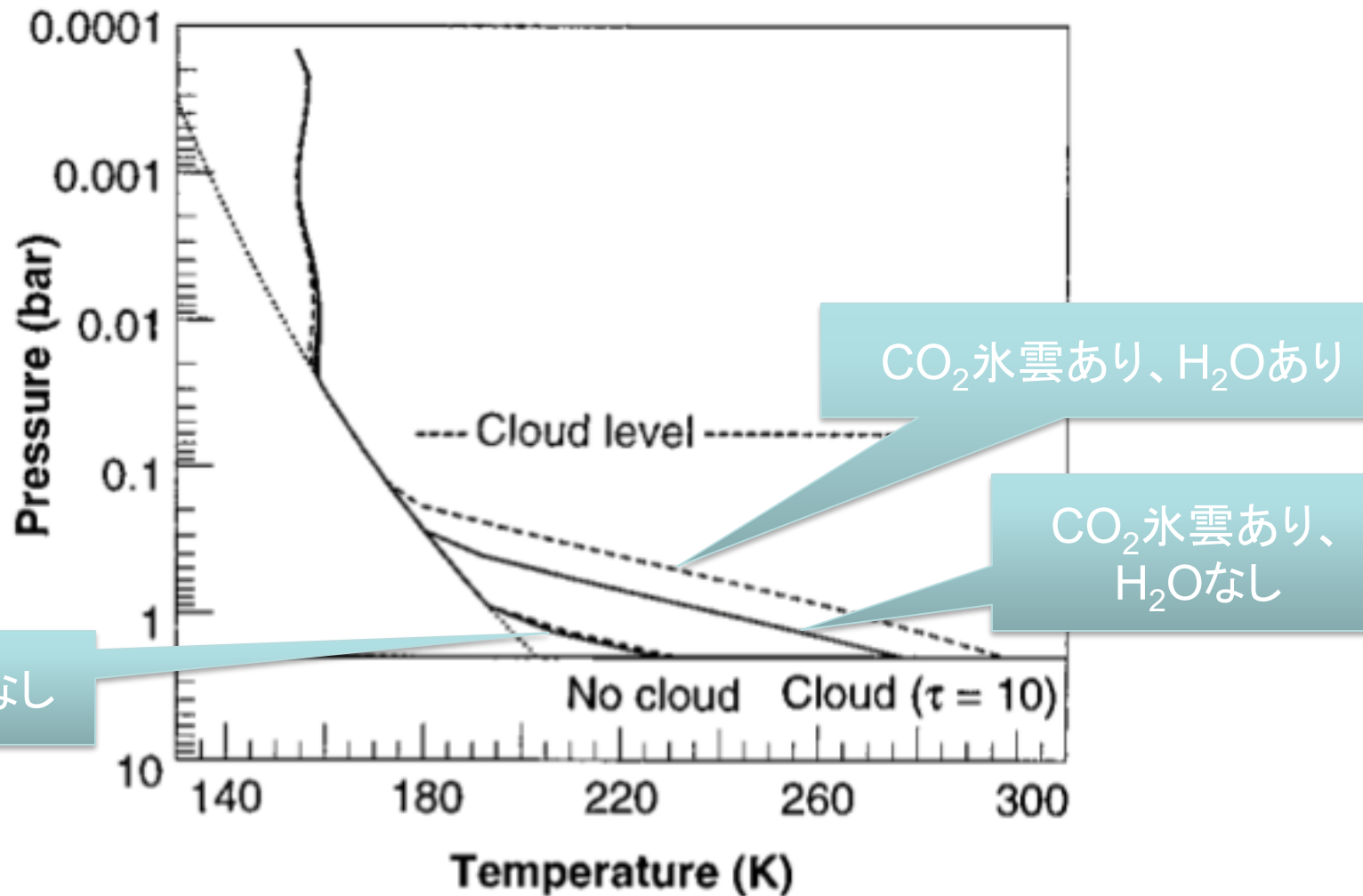


# 初期火星のCO<sub>2</sub>氷雲による温室効果

Forget & Pierrehumbert (Science, 1997)

- CO<sub>2</sub>氷雲は赤外線をよく散乱する。そのため地表から宇宙に向けて発せられる熱放射を散乱して地表に戻し、温室効果をもたらす。
- CO<sub>2</sub>氷雲は太陽光に対するアルベド(反射率)を大きくして大気を冷却する働きもあるが、厚いCO<sub>2</sub>大気の場合にはもともと大気そのもののアルベドが大きいので、CO<sub>2</sub>氷雲がもたらす温室効果による加熱の寄与が勝る。
  - たとえば2気圧の雲無しCO<sub>2</sub>大気はアルベド0.38を持つ。ここにCO<sub>2</sub>氷雲を加えてアルベドが0.65となり太陽光吸収量が40%減るとき、CO<sub>2</sub>氷雲は宇宙に出て行く赤外放射を60%減らす。(このような雲は可視光に対する光学厚さ10に相当する)

2気圧のCO<sub>2</sub>大気、光学厚さ10のCO<sub>2</sub>氷雲、現在の火星軌道の太陽光量の75%を仮定したときの温度構造



→ 1-2気圧のCO<sub>2</sub>大気があれば0°C以上になりそう

# **3D modelling of the early martian climate under a denser CO<sub>2</sub> atmosphere: Temperatures and CO<sub>2</sub> ice clouds**

(Forget et al. 2013, Icarus)

- 3D global climate simulations of the early martian climate performed assuming a faint young Sun and a CO<sub>2</sub> atmosphere with surface pressure between 0.1 and 7 bars
- Previous studies had suggested that CO<sub>2</sub> ice clouds could have warmed the planet thanks to their scattering greenhouse effect. However, even assuming parameters that maximize this effect, it does not exceed +15 K. As a result, a CO<sub>2</sub> atmosphere could not have raised the annual mean temperature above 0 ° C anywhere on the planet.
- This is consistent with a cold early Mars scenario in which nonclimatic mechanisms must occur to explain the evidence for liquid water.

# Role of thick CO<sub>2</sub> atmosphere

- It has been suggested that a 5-bar CO<sub>2</sub> atmosphere would raise the global mean surface temperature to 0 ° C or more, allowing “warm and wet” conditions.
- At higher pressures CO<sub>2</sub> can condense in the middle atmosphere. This decreases the greenhouse effect because of the latent heat warming of the middle atmosphere, which leads to cooling of the lower atmosphere. Furthermore the resulting CO<sub>2</sub> ice clouds would raise the planetary albedo and further cool the planet.
- **Assuming that the CO<sub>2</sub> ice cloud particles are larger than a few micrometers**, they can readily scatter infrared radiation and reflect outgoing thermal radiation back to the surface. The resulting ‘scattering greenhouse’ effect will warm the surface.

# Model

- 3-D Global Climate Model
- Surface temperature evolution is governed by the balance between radiative and sensible heat fluxes (direct solar insolation, thermal radiation from the atmosphere and the surface, and turbulent fluxes) and thermal conduction in the soil.
- Parameterization to account for the condensation of CO<sub>2</sub> on the ground and in the atmosphere (CO<sub>2</sub> ice clouds).
- To estimate the size of the cloud particles, we assumed that the number mixing ratio of cloud condensation nuclei [CCN] is constant throughout the atmosphere.
- To explore the impact of atmospheric dust on the early Mars climate, we added a second type of aerosol in addition to the CO<sub>2</sub> ice clouds particles.

# Mean surface temperature vs. Surface pressure (column CO<sub>2</sub> amount)

- Surface temperature increases up to 2 bar. Above 2–3 bar Rayleigh scattering by CO<sub>2</sub> gas more than compensates for the increased thermal infrared opacity of the atmosphere. Increasing the atmospheric thickness does not result in an increase of the mean surface temperature.
- Taking into account the radiative effect of CO<sub>2</sub> ice clouds results in a global warming of the surface by more than 10 K resulting from the CO<sub>2</sub> ice cloud scattering greenhouse effect.
- The collapse of the atmosphere into permanent CO<sub>2</sub> ice caps is predicted for pressures higher than 3 bar.

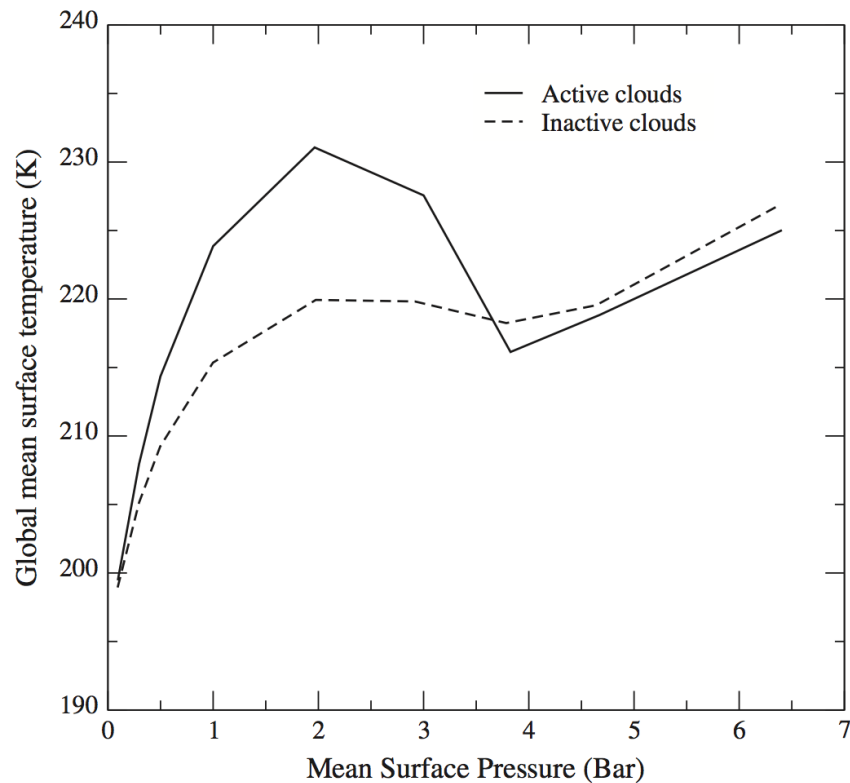
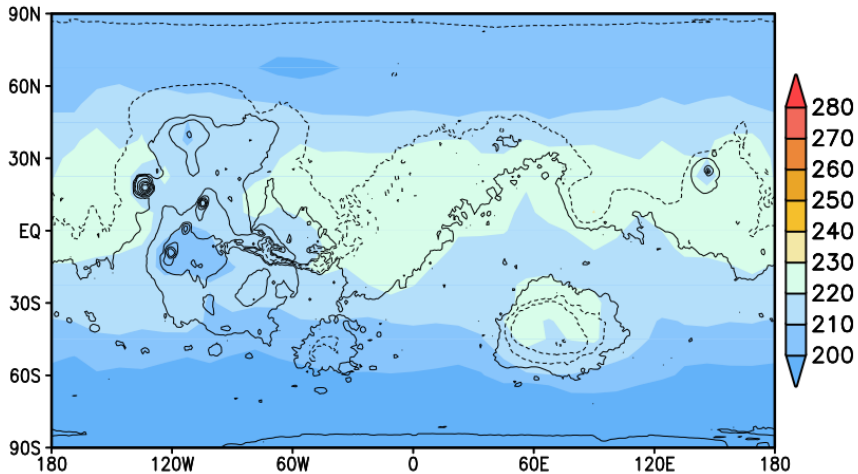


**Fig. 1.** Global mean annual mean surface temperature (K) as a function of surface pressure in our baseline simulations (obliquity = 25°, [CCN] =  $10^5 \text{ kg}^{-1}$ , circular orbit) with and without radiatively active CO<sub>2</sub> ice clouds.

# Surface temperatures for present-day ground albedo (0.22)

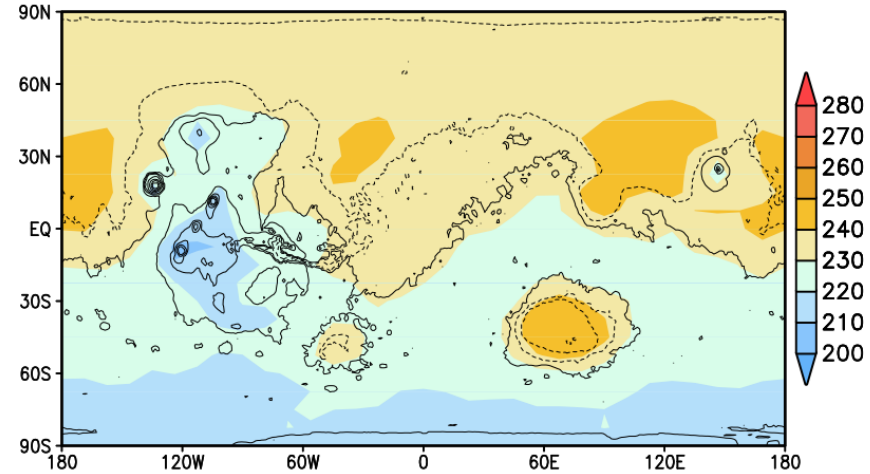
**Ps=0.5 bars**

(a) Annual mean temperatures (K)

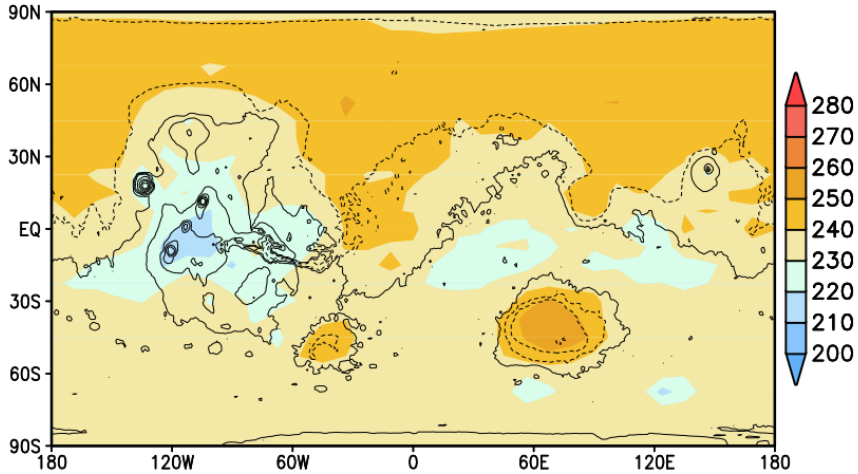


**Ps=2 bars**

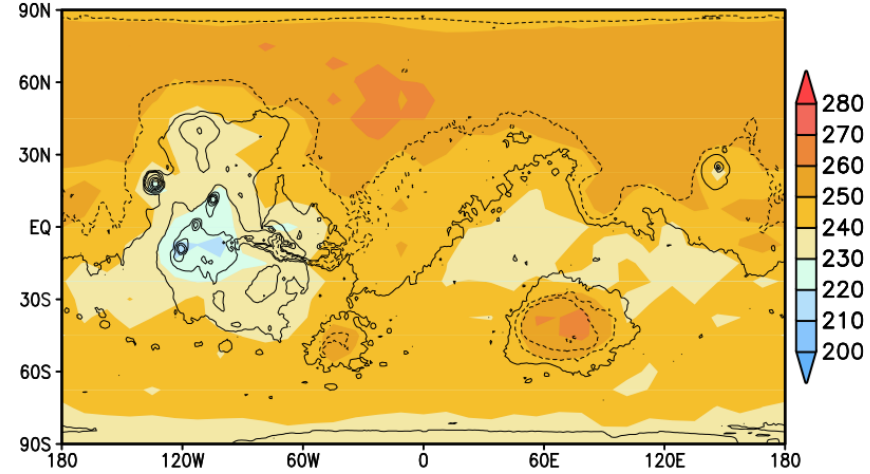
(b) Annual mean temperatures (K)



(c) Max daily mean temperatures (K)



(d) Max daily mean temperatures (K)

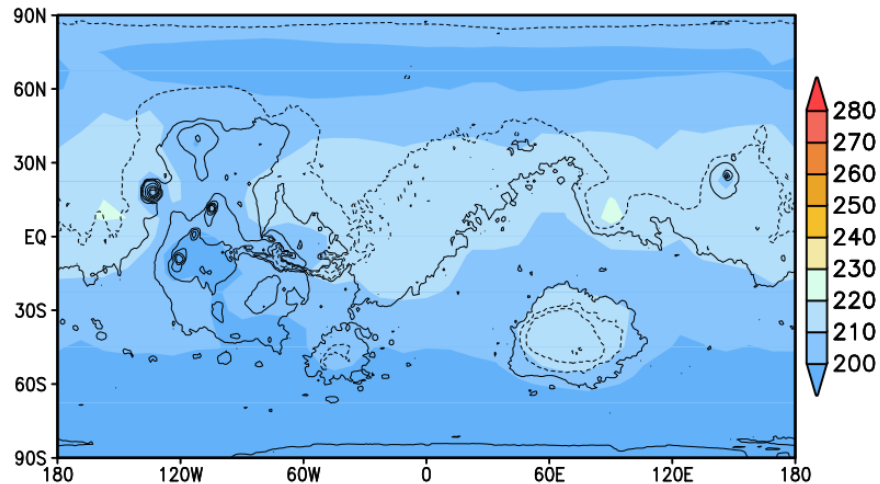


- annual mean surface temperatures are always significantly below 0 ° C.

# Surface temperatures for ice-covered ground albedo (0.4)

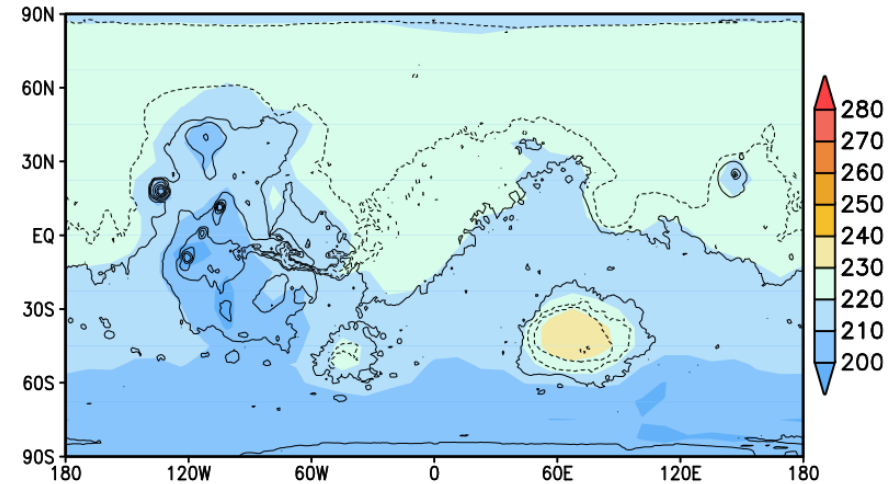
**Ps=0.5 bars**

(a) Annual mean temperatures (K)

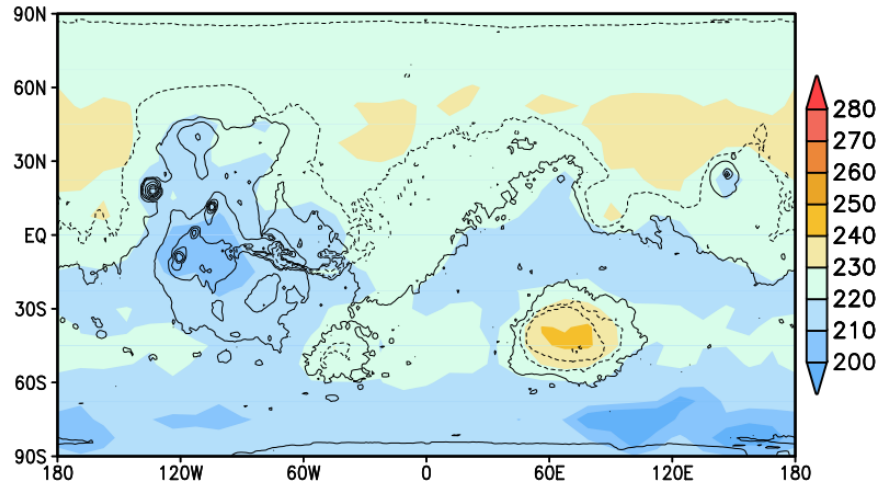


**Ps=2 bars**

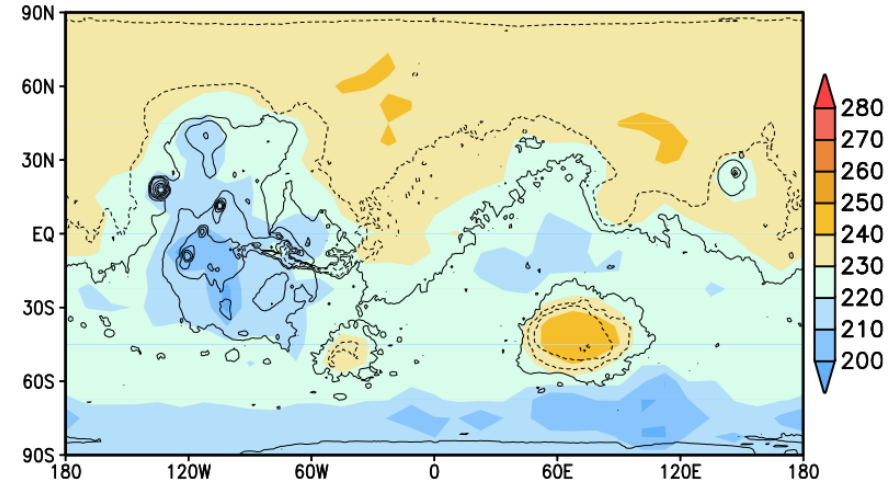
(b) Annual mean temperatures (K)



(c) Max daily mean temperatures (K)



(d) Max daily mean temperatures (K)

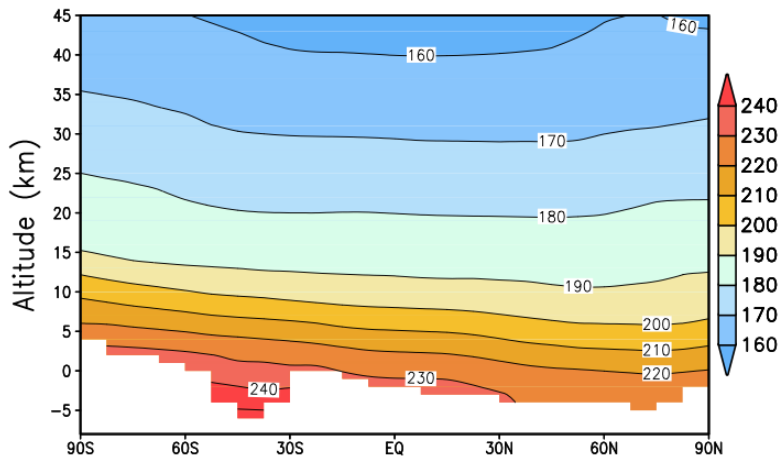


- annual mean surface temperatures are always significantly below 0 ° C.

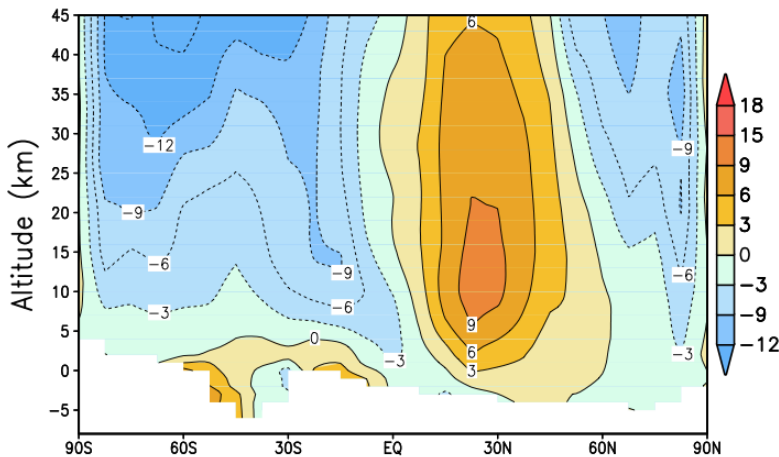
# Meridional cross section

**Northern Winter** ( $L_s = 270^\circ - 300^\circ$ )

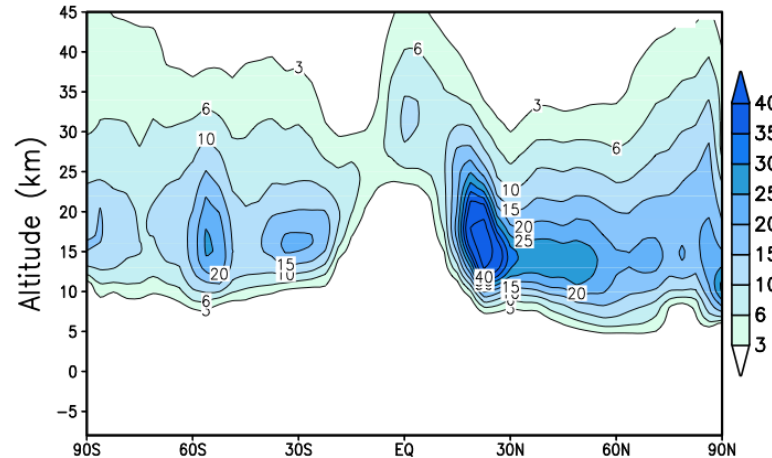
(b) Zonal mean temperatures (K)



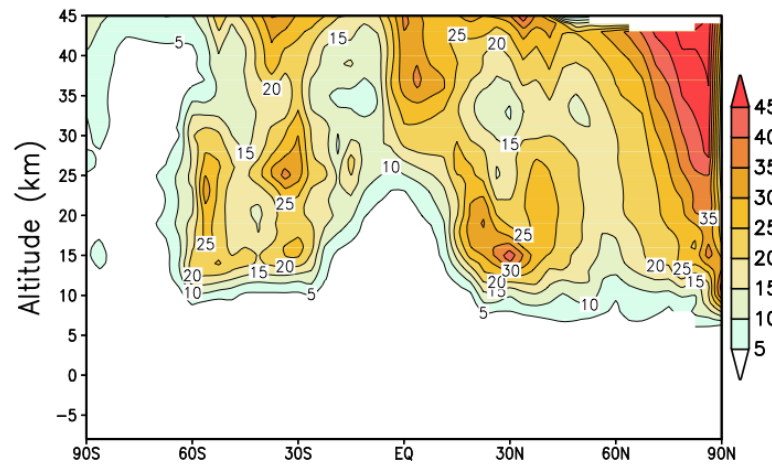
(d) Zonal mean zonal wind ( $\text{m s}^{-1}$ )



(b) Zonal mean  $\text{CO}_2$  ice density ( $10^{-6} \text{ kg m}^{-3}$ )

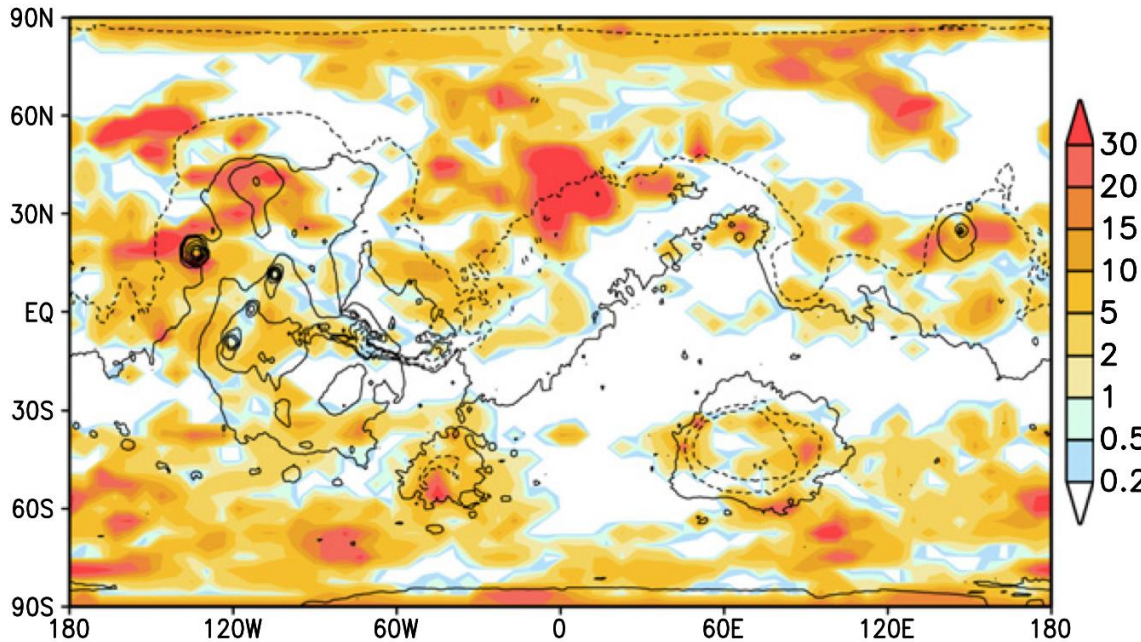


(d) Mean Cloud particles effective radius ( $\mu\text{m}$ )



- temperatures below the  $\text{CO}_2$  condensation point are predicted above about 11 km, and  $\text{CO}_2$  ice clouds form at all seasons and latitudes

# An example of the instantaneous CO<sub>2</sub> ice clouds coverage for a mean surface pressure 2 bar



- CO<sub>2</sub> ice clouds cover a major part of the planet but not all. Their behavior is controlled by a combination of large scale ascents and descents of air, stationary and travelling waves, and resolved gravity waves related to the topography.
- The mean cloud warming remains lower than 15 K because of the partial cloud coverage and the limited cloud optical depth.

**CO<sub>2</sub> ice clouds visible opacity,  $L_s = 270^\circ$ , noon at 0°E**

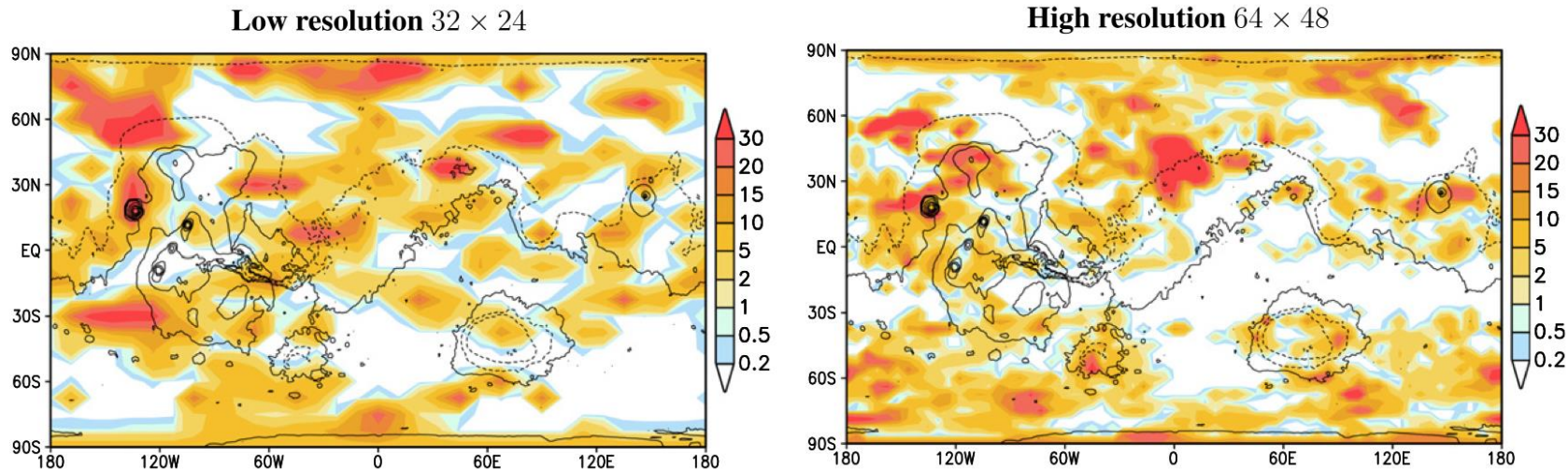


**Fig. 11.** An example of the instantaneous CO<sub>2</sub> ice clouds coverage for two simulations with different horizontal resolution (mean surface pressure 2 bar, obliquity = 25°, [CCN] = 10<sup>5</sup> kg<sup>-1</sup>, circular orbit).

average visible opacity ~ 4.5

- A CO<sub>2</sub> atmosphere could not have raised the annual mean temperature above 0° C anywhere on the planet. The collapse of the atmosphere into permanent CO<sub>2</sub> ice caps is predicted for pressures higher than 3 bar.
- Consistent with a cold early Mars scenario in which nonclimatic mechanisms must occur to explain the evidence for liquid water.

# Unsolved issue: cloud condensation nuclei (CCN)

- CCN is a key parameter which directly controls the properties and the impact of the modeled clouds. This parameter is poorly known.
- Even in the absence of surface or chemical sources, a minimum number of nuclei would be provided by meteoritic dust.

# Unsolved issue: Early Sun

- The gradual increase in luminosity during the core hydrogen burning phase of evolution of a star is an inevitable consequence of Newtonian physics and the functional dependence of the thermonuclear reaction rates on density, temperature and composition.
- The only way to explain a brighter early Sun is to assume that it was more massive initially and that it subsequently lose the excess mass in an intense solar wind during its first billion years.
- A younger more massive Sun has also been suggested recently

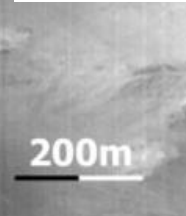
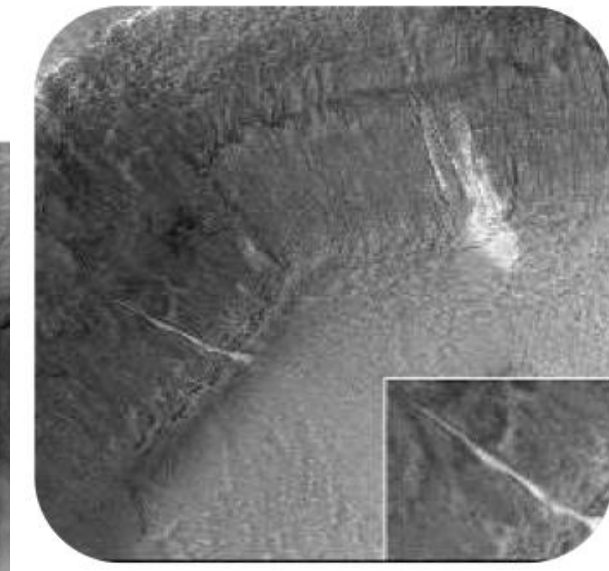
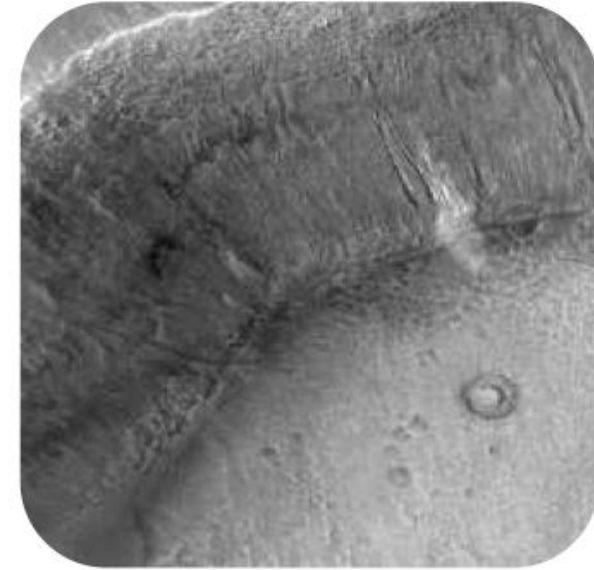
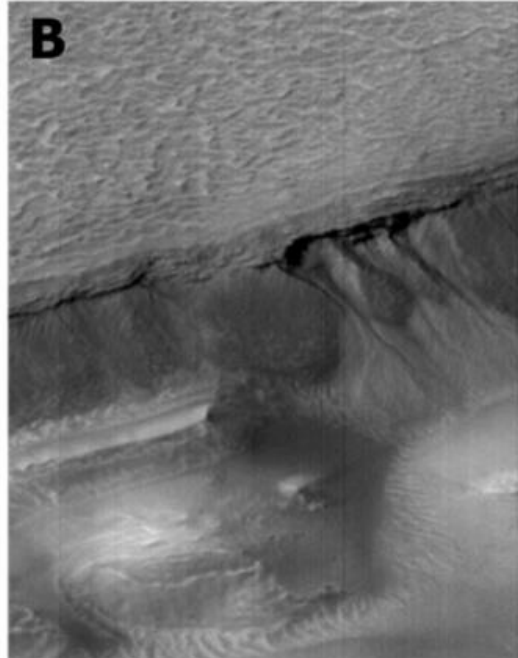
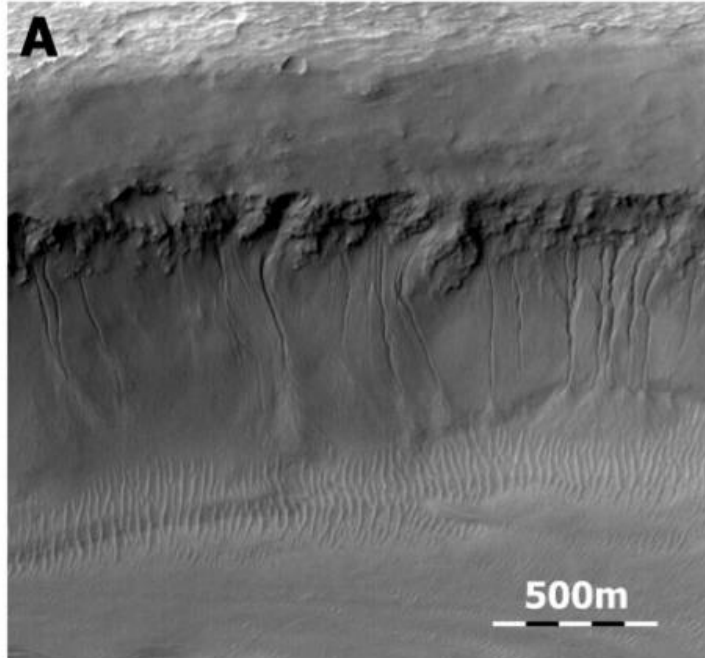
# Unsolved issue: Other greenhouse gases

- Ammonia ( $\text{NH}_3$ ) : 500 ppm of  $\text{NH}_3$  in a 4–5 bar  $\text{CO}_2$  atmosphere could raise surface temperatures to 273 K. However,  $\text{NH}_3$  is photochemically unstable and would require shielding to survive.
- Methane ( $\text{CH}_4$ ) : even at concentrations of 500 ppm  $\text{CH}_4$  does not significantly boost the greenhouse effect of a pure  $\text{CO}_2/\text{H}_2\text{O}$  atmosphere.  $\text{CH}_4$  would require strong sources to sustain the above concentrations.
- Sulfur dioxide ( $\text{SO}_2$ ) & hydrogen sulfide ( $\text{H}_2\text{S}$ ) : An obvious source for these gases is volcanic activity.  $\text{SO}_2$  needs to build up to concentrations around the 10 ppm level or higher.  $\text{SO}_2$  readily converts to aerosols, and these aerosols should have a net cooling effect on surface temperatures. Furthermore,  $\text{SO}_2$  is highly soluble and will washout quickly when conditions become warm enough for rainfall.

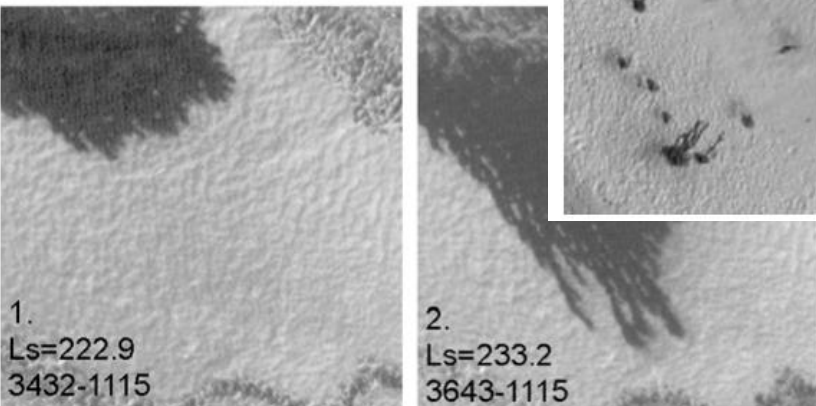
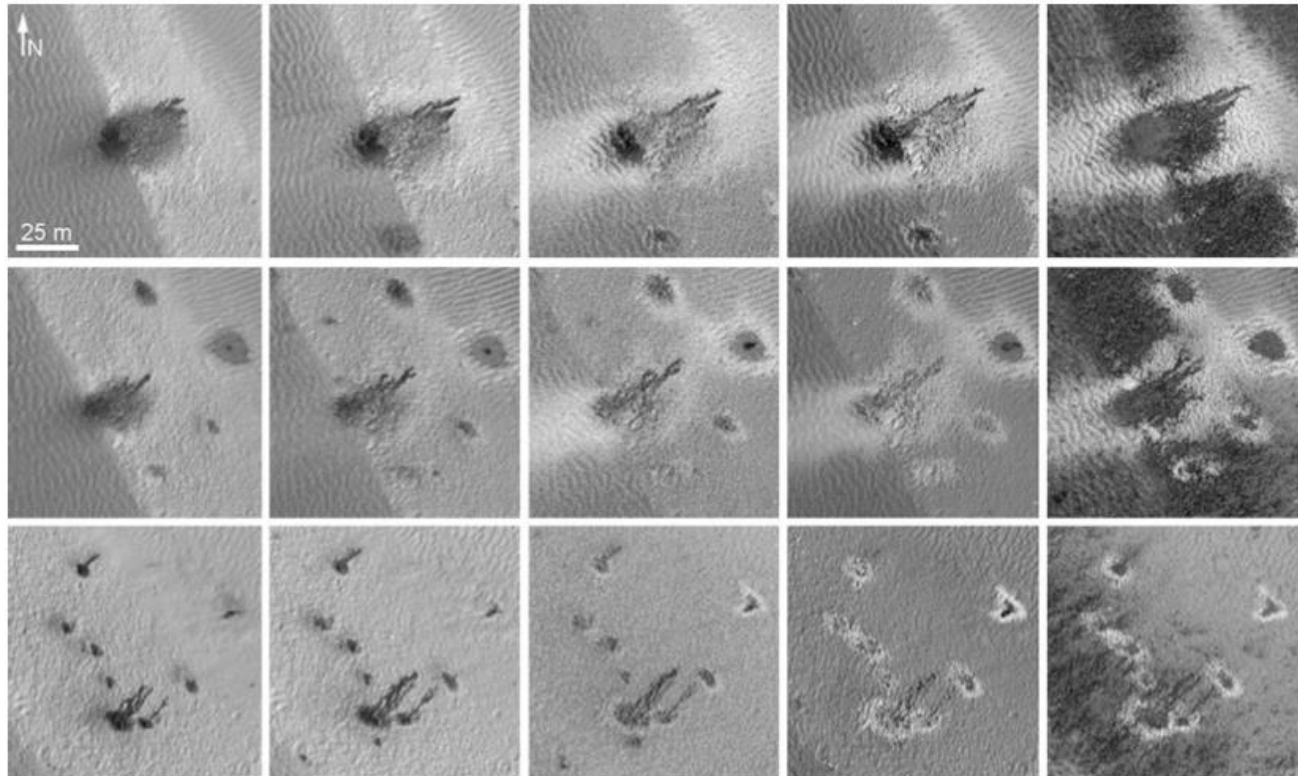
# 火星の水の多様な姿

- なぜここで液体の水が流れるのか

Gullies

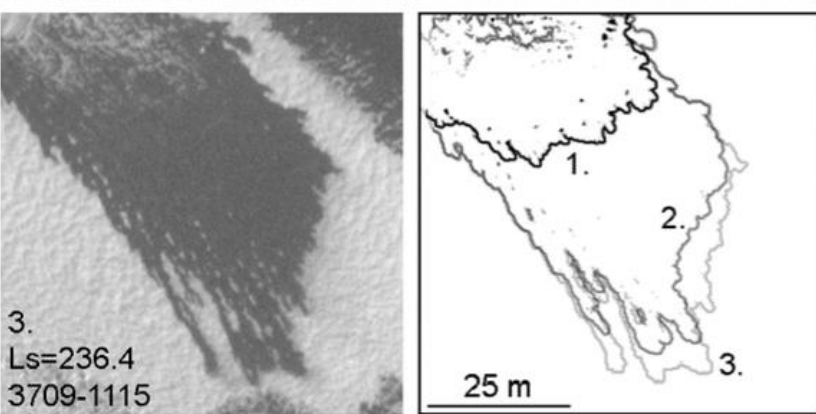


## Seepages



1.  
 $L_s=222.9$   
3432-1115

2.  
 $L_s=233.2$   
3643-1115

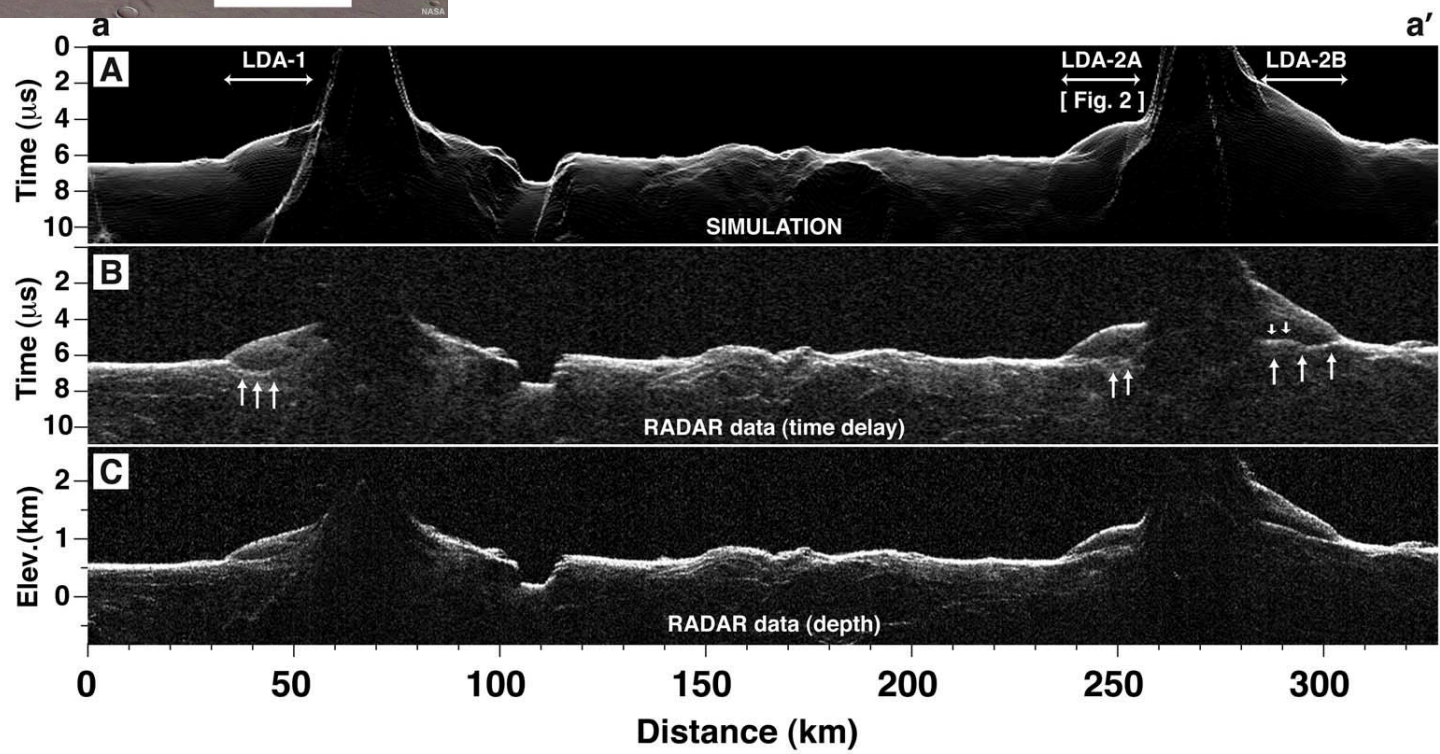


3.  
 $L_s=236.4$   
3709-1115

- 現在の火星気候は平衡状態と言えるのかどうか

White collars

# Buried glaciers

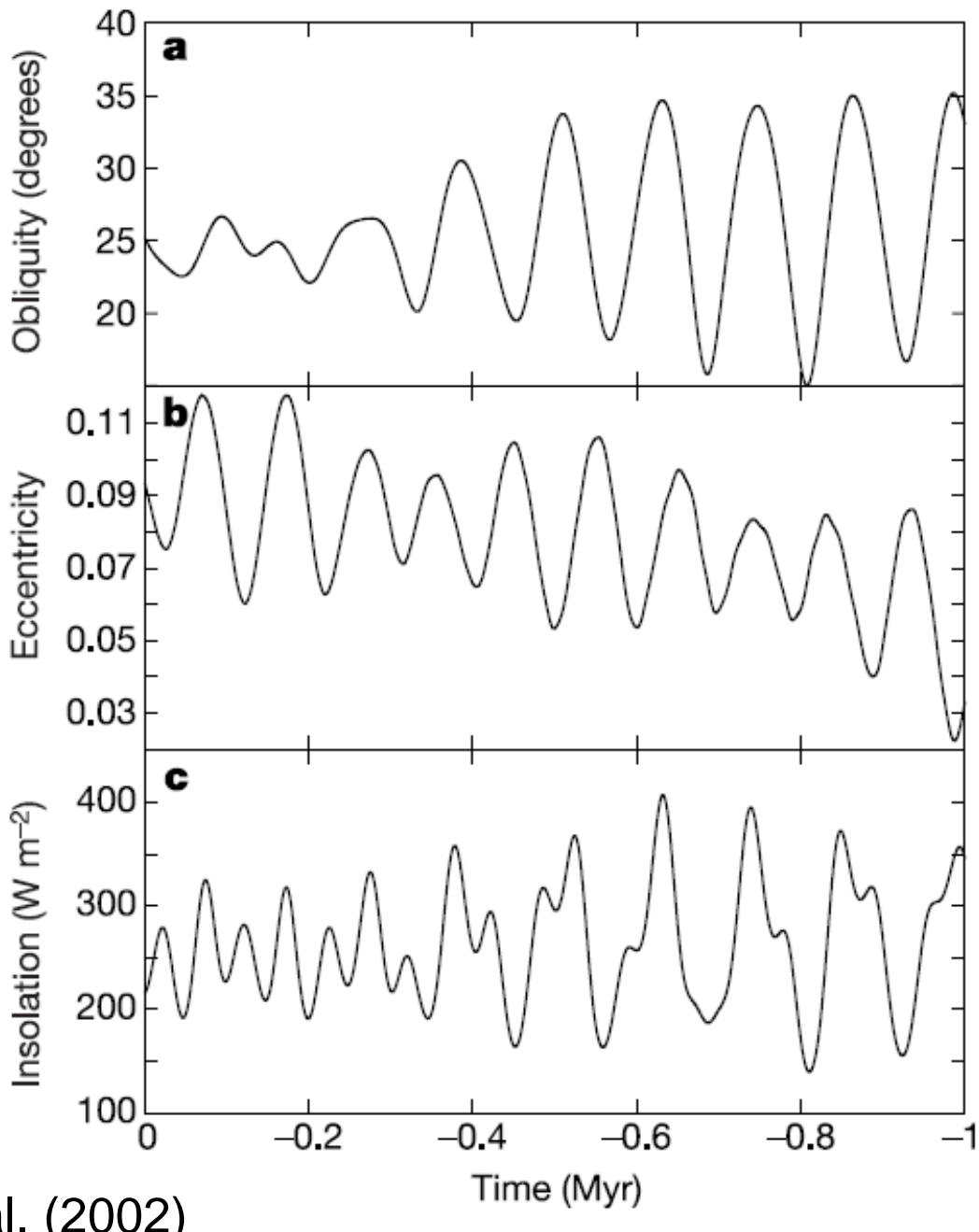


# 天体力学的強制

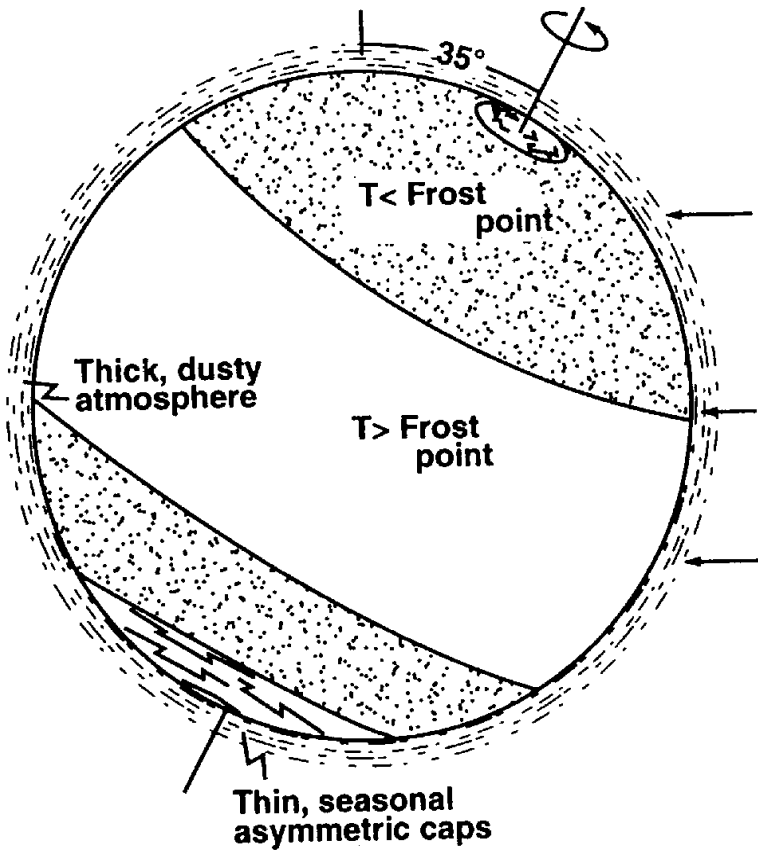
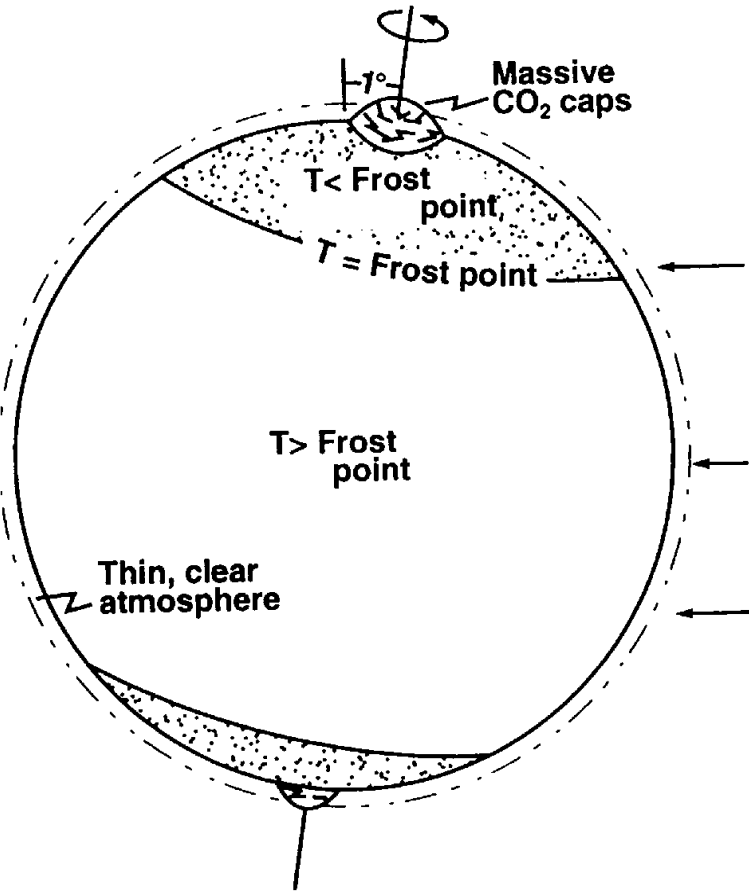
自転軸傾斜角

軌道離心率

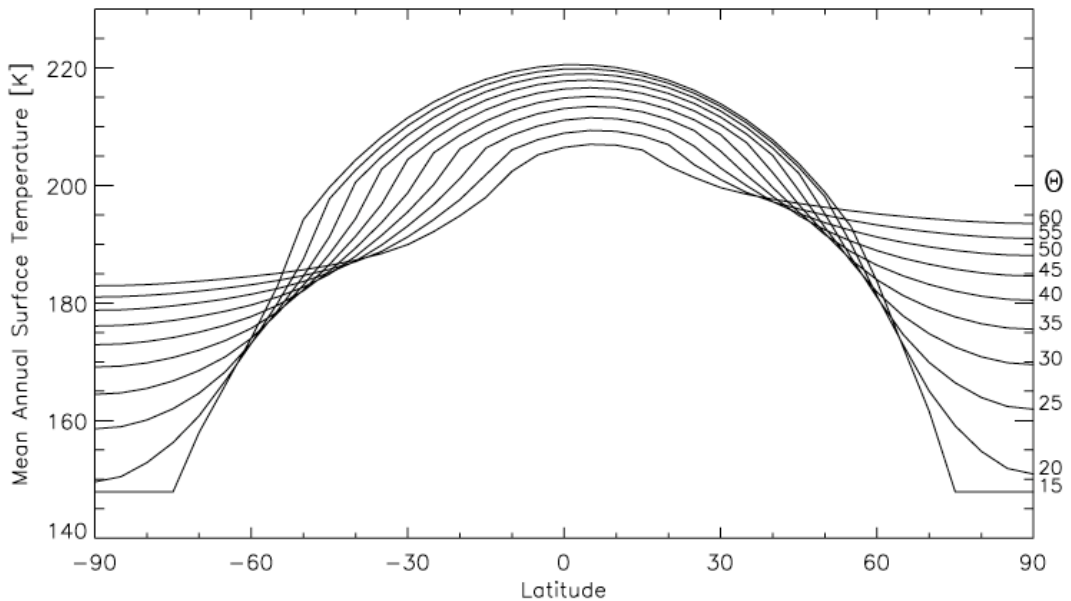
北極域の夏至の日射



Laskar et al. (2002)

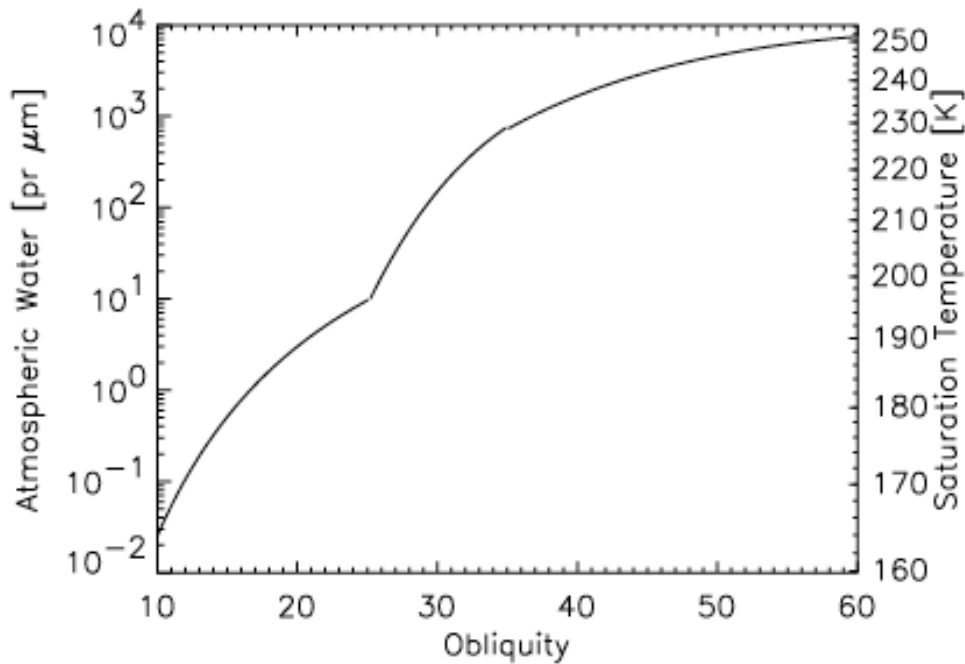


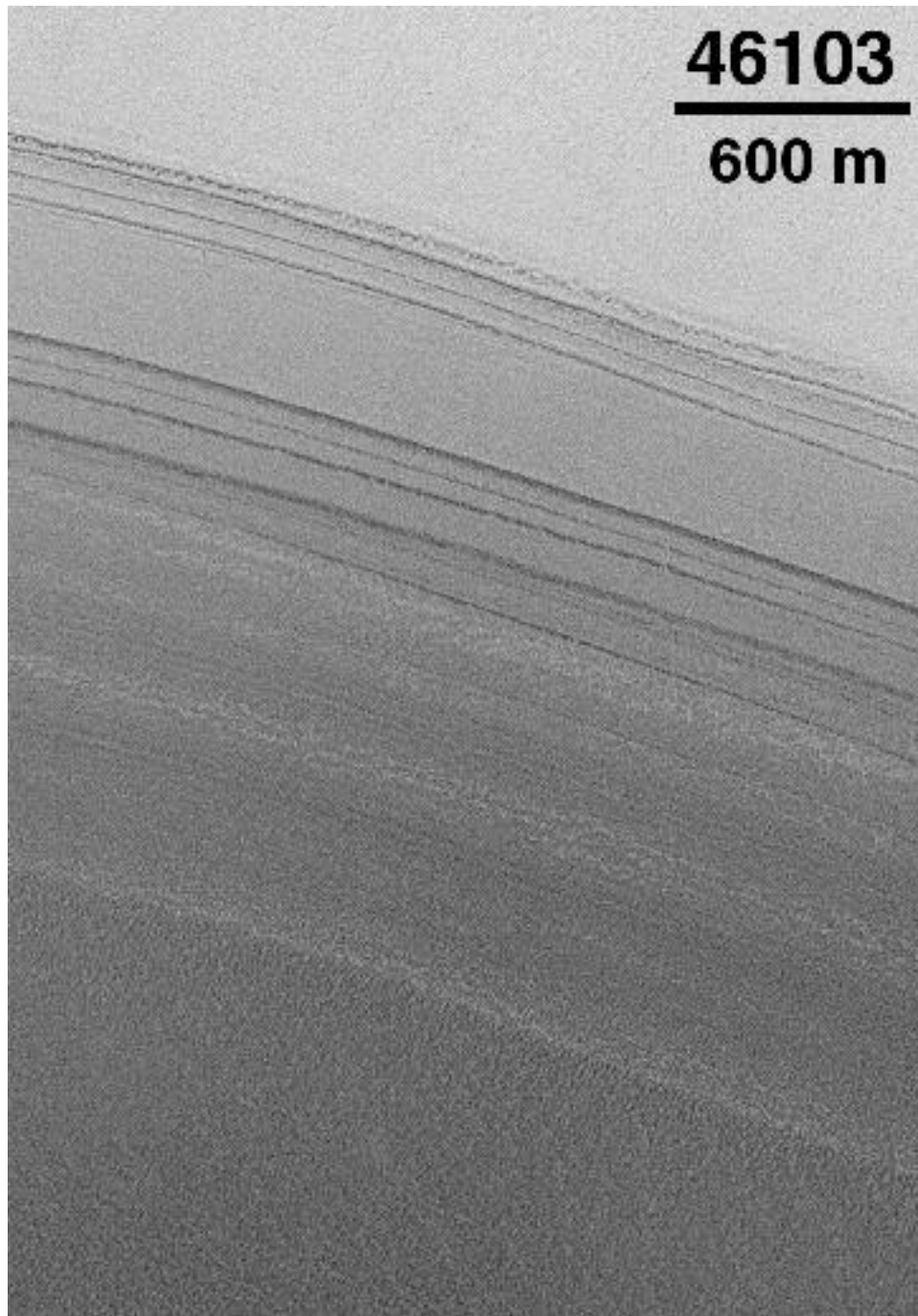
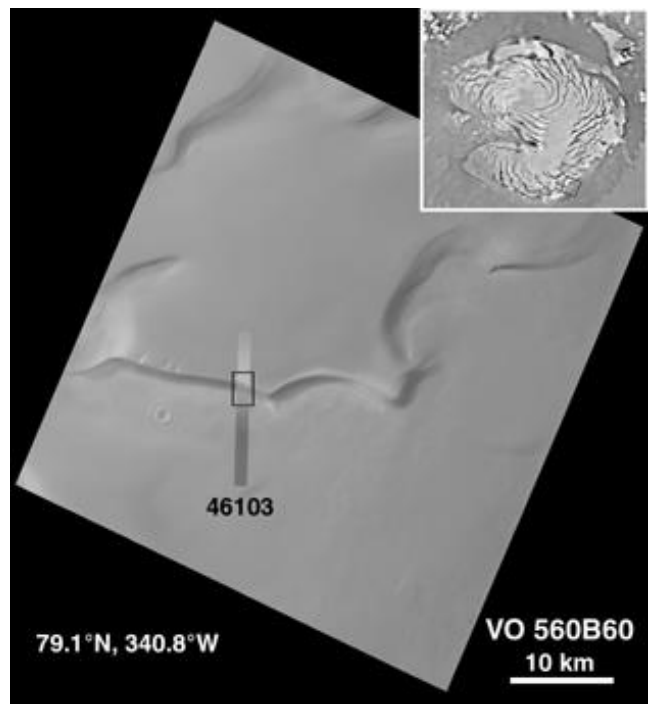
- **自転傾斜角が小さくなる**→極域が寒冷化→水蒸気が極域に凝結(夏にもCO<sub>2</sub>氷に覆われて蒸発しない)→全球的に水蒸気濃度低下→**氷床が高緯度に後退**
- **自転傾斜角が大きくなる**→極域が温暖化→水蒸気が極域から蒸発→全球的に水蒸気濃度上昇→**氷床が低緯度まで張り出す**



**Figure 3.** Mean annual surface temperature for a range of obliquities. The eccentricity is 0.12, and the  $L_S$  at which perihelion occurs is 270, corresponding to southern summer. A thermal inertia of  $250 \text{ J m}^{-2} \text{ s}^{-1/2} \text{ K}^{-1}$ , an albedo of 0.25, a surface pressure of 600 Pa, and an infrared dust opacity of 0.1 are assumed. Discontinuities in the slope of each curve are due to the effects of seasonal CO<sub>2</sub> frost.

Mellon & Phillips (2001)

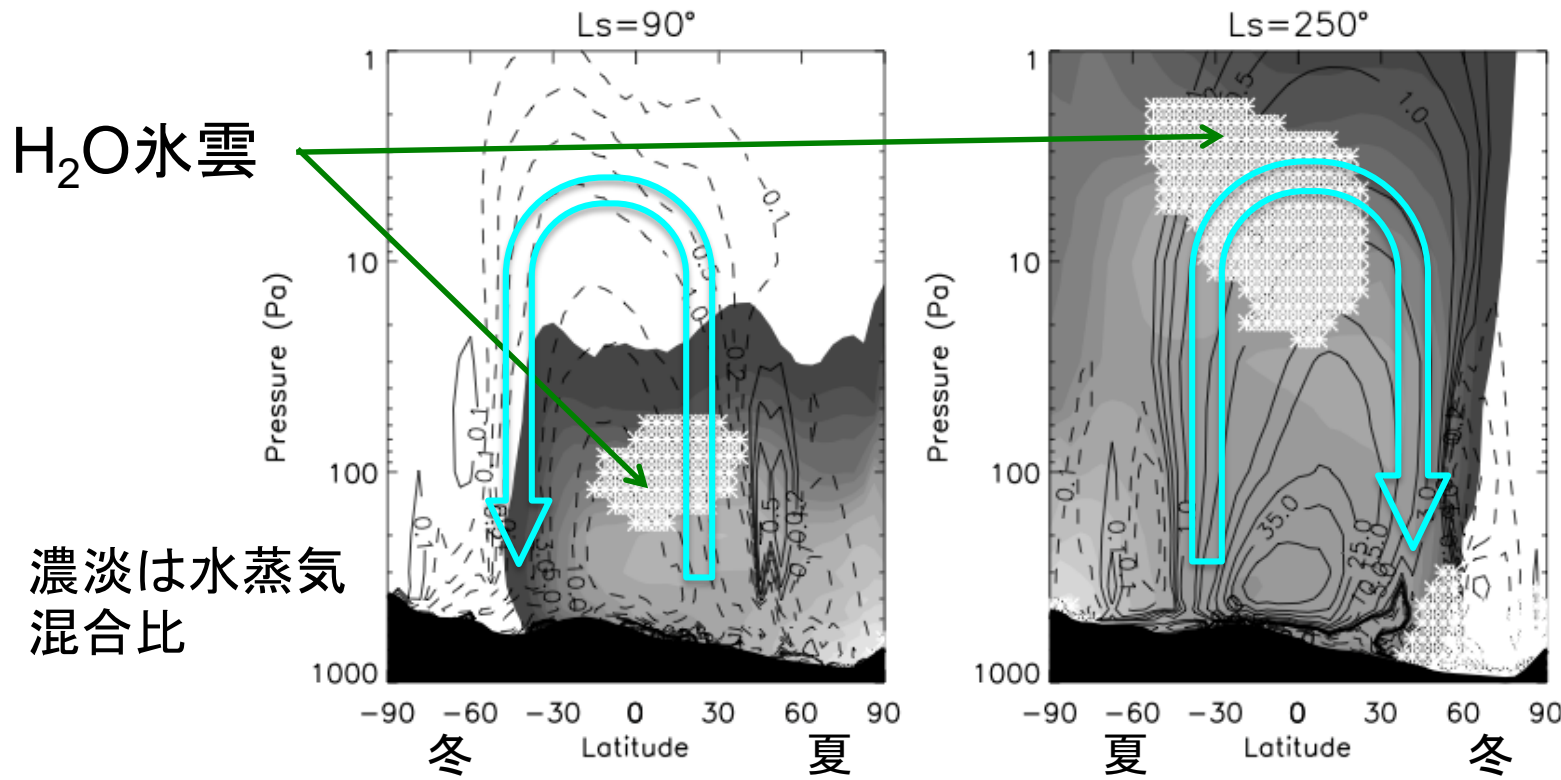




極冠堆積物

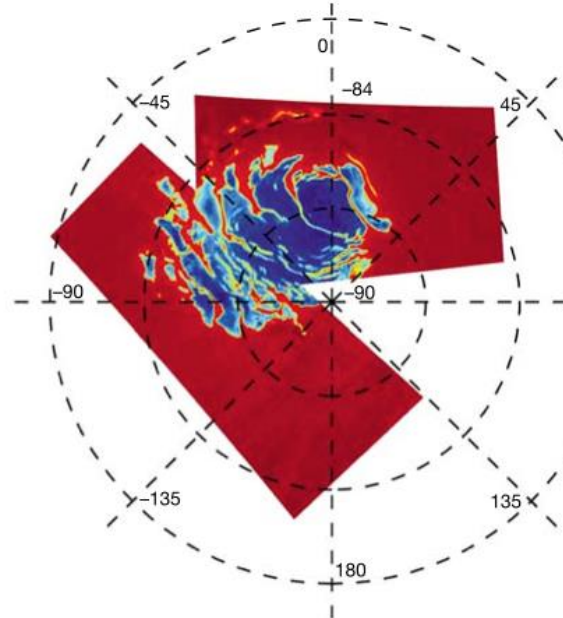
## ハドレー循環による水輸送

- 南半球の夏のほうが北半球の夏より暖かいため、夏半球から冬半球への水蒸気輸送が、南半球の夏に効率よく起こる。
  - 年間積算では北極域に水を集める傾向がある。

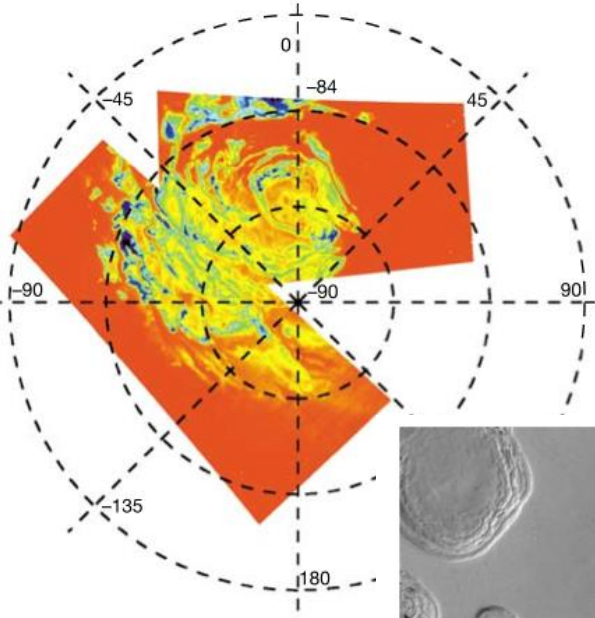


# Permanent CO<sub>2</sub> cap at the South pole

青いところにCO<sub>2</sub>氷



青いところにH<sub>2</sub>O氷



浸食されつつある残存  
CO<sub>2</sub>極冠の一部

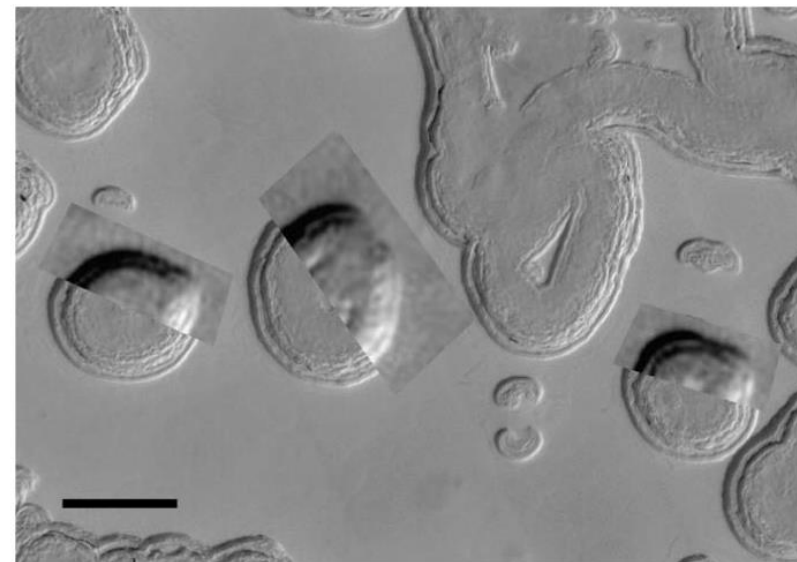


Figure 1 Global maps of CO<sub>2</sub> and H<sub>2</sub>O ices at the south pole of Mars. Left, the CO<sub>2</sub>-ice absorption feature is scaled from blue (deep) to brown (CO<sub>2</sub>-ice-free areas); right, mapping of the H<sub>2</sub>O ice, from blue (deep absorption) to red (ice-free). Comparison shows that the H<sub>2</sub>O-ice areas extend far beyond the CO<sub>2</sub> isolated units tens of kilometres wide.

Bibring et al. (2004)

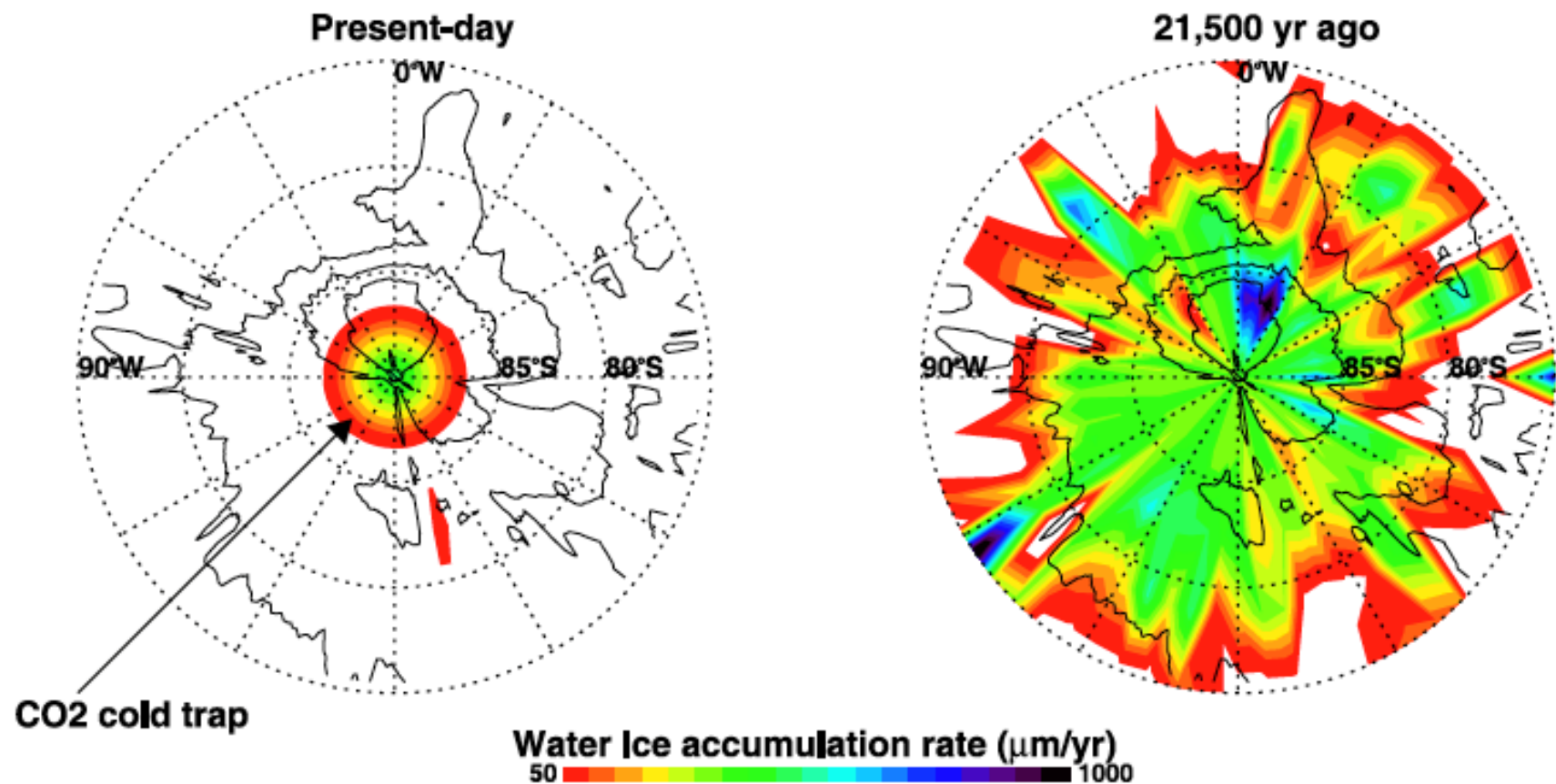
CO<sub>2</sub>残存極冠のおかげで  
残存H<sub>2</sub>O氷も存在か

Fig. 8. Three year changes in unit B. Registered clips from MOC image E11-01220 superposed on HiRISE image PSP\_004744\_0870. Note that the three year change includes one or two ridges interior to the present depression edge. Illumination in MOC images from upper left, in HiRISE more from the left. MOC  $L_s = 286^\circ$ , HiRISE  $L_s = 287^\circ$ . Scale bar 50 m. Centered at 86.9°S, 89.4°W.

- Water in the southern polar cap : remnant from the past where the southern water ice was stable?
- How stable is the current southern water ice cap?



Montmessin et al. (2007)



**Figure 5.** A comparison of water ice accumulation rates predicted by the model in the south polar region for the two perihelion configurations. Present-day map shows net accumulation only at the south pole itself (equivalent to 1 grid point in the model) where the prescription of a CO<sub>2</sub> cold trap forces a local and permanent deposition of water ice. In the reversed perihelion simulation (Figure 5, right), the CO<sub>2</sub> cold trap has been removed and the pattern of accumulation is only controlled by a precipitation versus sublimation positive balance on an annual average.

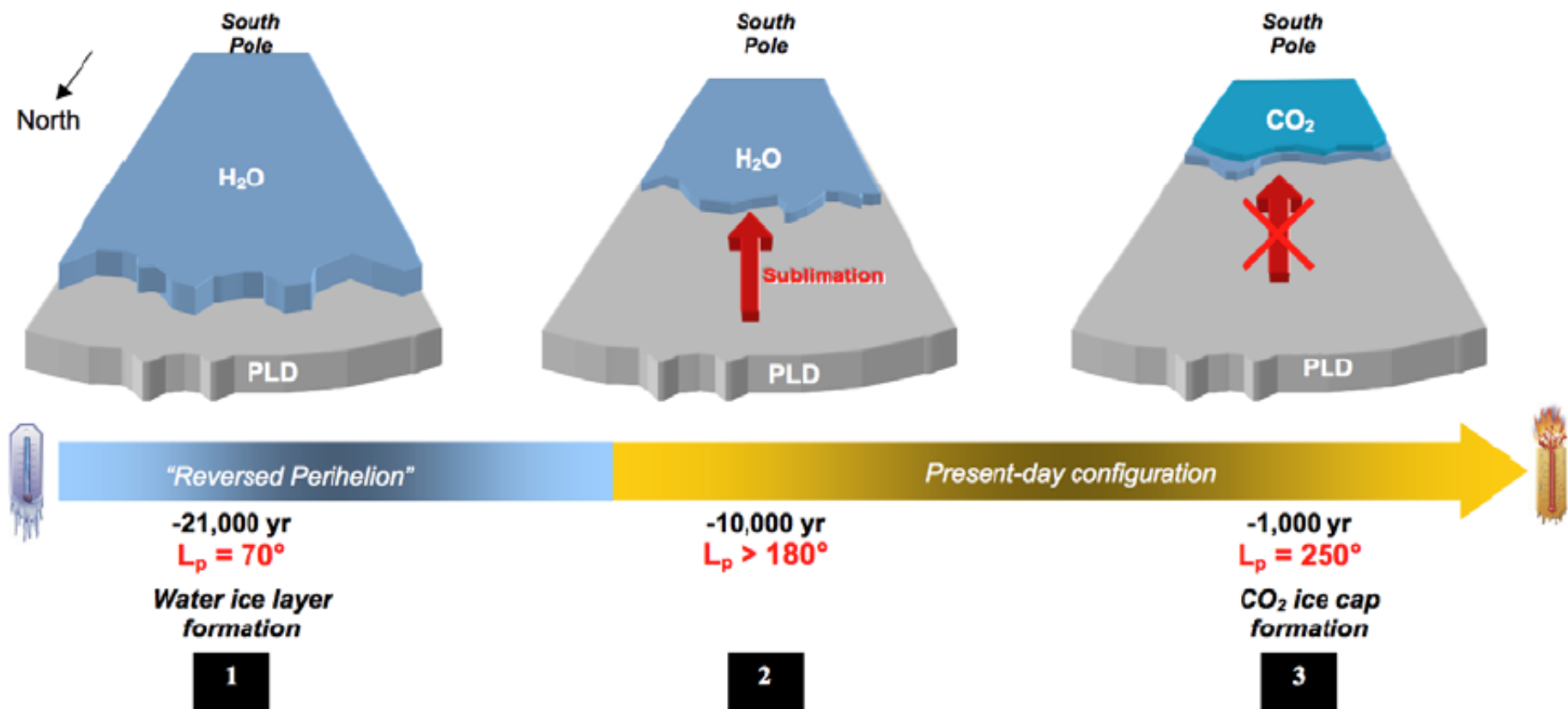
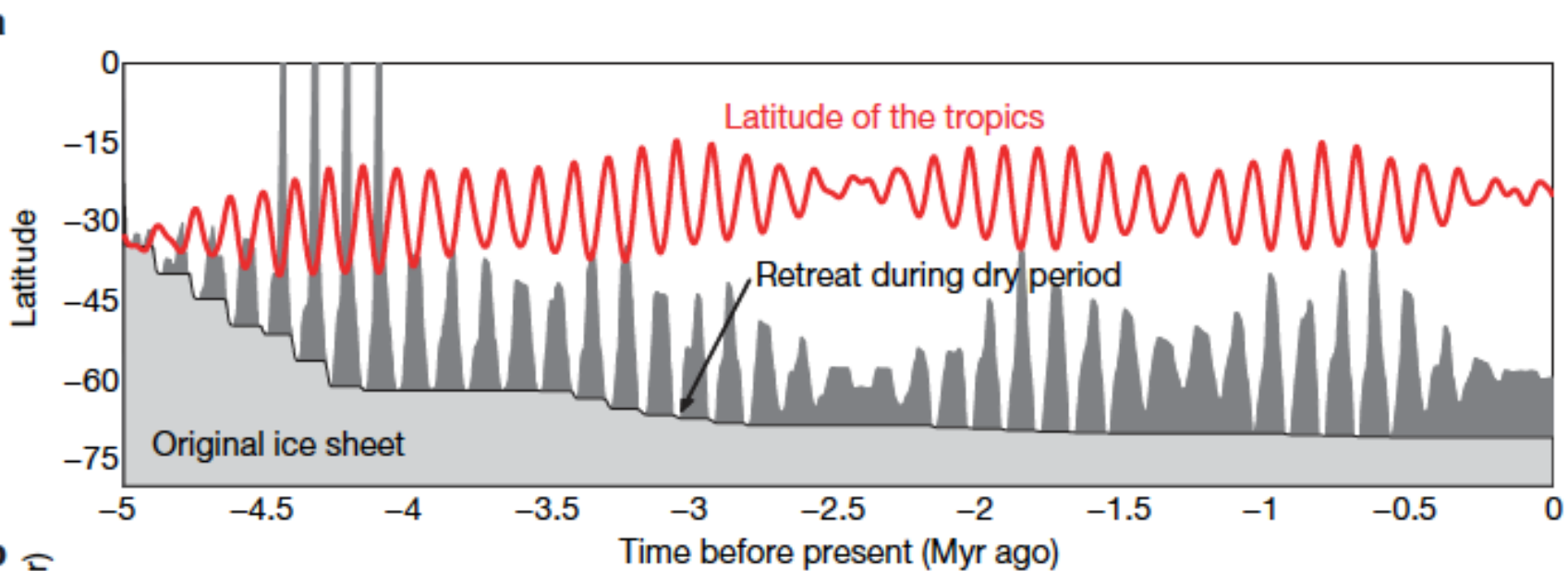


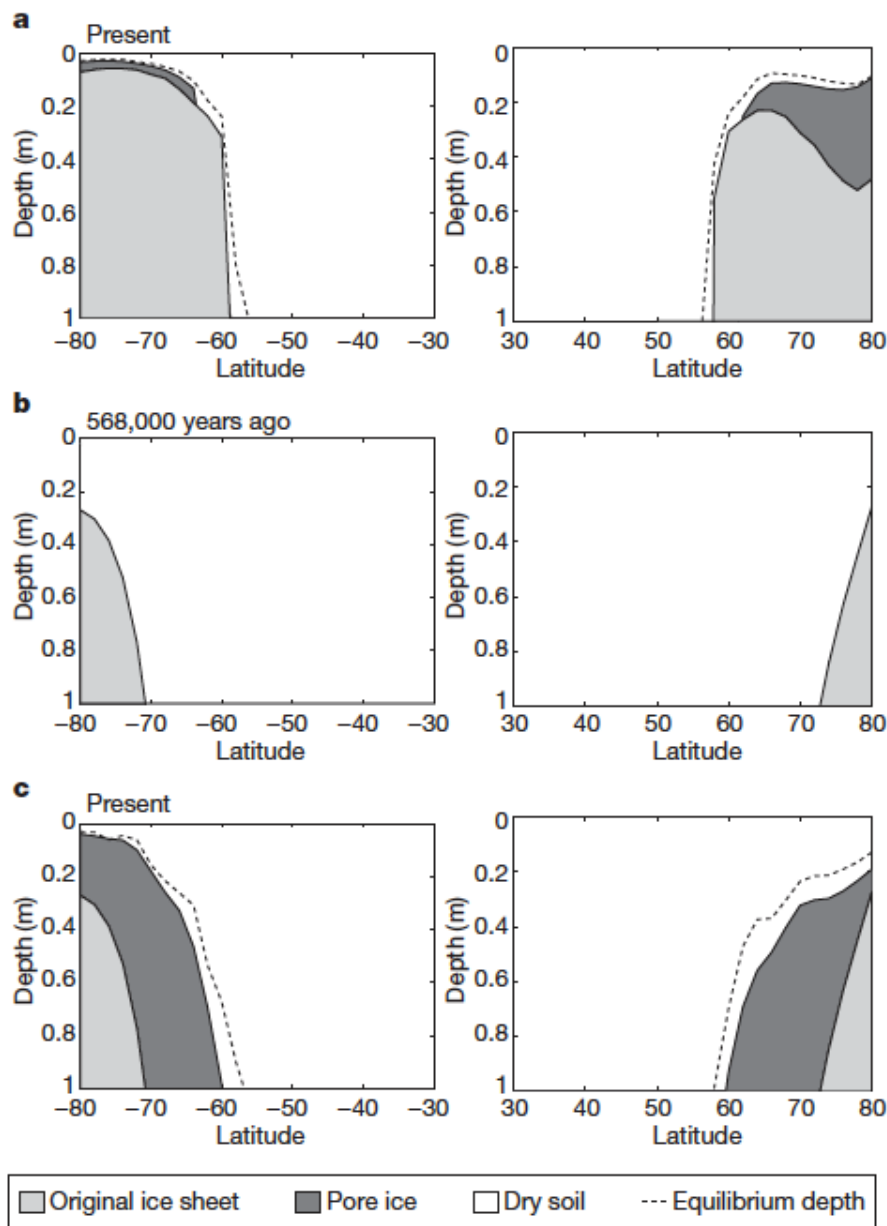
**Figure 9.** Illustration summarizing the sequence of events in the south polar region since the last reversed perihelion regime of the precession cycle. At event 1 time, water was extracted off the north polar cap and was deposited over the south PLD terrains thanks to a favorable summer insolation gradient between the poles. For event 2, passage to present-day configuration, with perihelion argument now entering a northern spring regime, reversed the orientation of the insolation gradient and forced water to progressively return back to the north pole. For event 3, in a third act, the erosion process stopped as permanent CO<sub>2</sub> ice slabs formed and kept water from subliming further.

# 過去数百万年の氷床の変動

Schorrghofer (2007)

- ある時期に低緯度まで雪が降り積もって氷床が形成されたとして、そこからスタート
- 大気中の水蒸気量と地表温度の変化を外部から強制として与える
- 最初の氷床がそのまま残っている成分(ice sheet)と、いったん蒸発して大気中の水蒸気となったあと再び地下に拡散で戻ってきた成分(pore ice)を区別





水蒸気濃度を変化させなかつた場合の現在の地下氷分布

水蒸気濃度を変化させた場合の最近の自転角傾斜角極小時

水蒸気濃度を変化させた場合の現在の地下氷分布

**Figure 1 | Snapshots of the vertical ice distribution from model calculations.** a, At present and with atmospheric humidity constant throughout history. b, For strongly varying atmospheric humidity, 568,000 years ago. c, For strongly varying atmospheric humidity, at present. Dashed lines show the present-day equilibrium depth.